Novel SiCNW-Si/SiO_x-graphite based composite anode materials for Li-ion battery

by

Archisman Ray

A thesis

presented to the University of Waterloo

in fulfillment of the

thesis requirement for the degree of

Master of Applied Science

in

Chemical Engineering

Waterloo, Ontario, Canada, 2018

Author’s declaration:

I hereby declare that I am the sole author of this thesis. This is a true copy of the thesis, including any required final revisions, as accepted by my examiners.

I understand that my thesis may be made electronically available to the public.

Abstract:

Over the past years, the extensive use of graphite as an anode material in a Li-ion battery (LIB) led to its commercialization and use as the standard anode material in a LIB. The use of graphite as an anode material in LIBs at present, remains a cause of concern primarily when used in large scale applications like in that of automotive and grid applications owing to its limited power density and specific capacity. This makes it a bottleneck and restricts its application as a potential anode candidate in the lucrative electric vehicle industry. From the material viewpoint, Si-based anode materials are an attractive candidate owing to their high energy-density of nearly 4200 mAh/g as compared to only 372 mAh/g for the graphite-based anode material. This work primarily concentrates on the fabrication, characterization and performance analysis of composite anode materials of SiCNW-Si/SiO_x-graphite, with the aim of modifying the LIB to deliver a higher energy and power density with superior electrochemical performance coupled with good cycle performance, improved long-term stability and capacity retention without necessarily compromising with the cost and safety. This would therefore allow a potential scale up to the EV and HEV industry and for grid applications. The silicon carbide nanowires (SiCNWs) present in the composite apart from imparting strength, also increased the overall conductivity of the as-prepared composites, while effectively buffering the volume change of the Si/SiO_x particles and preventing capacity fading by disintegration of active material by imparting strength to the composite electrode structure. Coal tar, which is an abundant by-product of the carbonization of coal possessing significant health and environmental hazards was effectively recycled and reused by incorporating it into the anode structure to form SiCNWs via a two-step growth mechanism. The use of the coal tar in LIB proves to be beneficial from both the economic and environmental view point.

A simple, unique, cost-effective and scalable method to synthesize SiCNW-Si/SiO_x-graphite composites using commercial SiO_x, NFG (natural flaked graphite) powder and coal tar was investigated. By exploiting the advantages of the excellent long-term stability of graphite, high capacity of SiO_x and the unique structure SiCNW, SiCNW-Si/SiO_x-graphite composites with a unique architecture comprising of clustered micro-nano sized Si/SiO_x particles and thread-like SiCNWs were synthesized. These particles were found to be homogeneously dispersed and encapsulated within the conductive graphite matrix. The synthesis process comprised of a mechanical milling process followed by thermal annealing at 1000°C in an inert argon atmosphere. A typical composite electrode containing 25% SiO_x,11 % coal tar and 60% graphite by weight, when used in a half cell against Li metal counter electrode exhibits excellent stability and a high reversible capacity of 760 mAh/g at 0.1 A/g post 500 cycles. In addition, it has an excellent reversible capacity retention of 87.6% with consistently high coulombic efficiency (99.75% after the fourth cycle and stable at ~99.87% for 500 cycles) and remarkable electrochemical performance. Even at higher rates ranging between 0.5-2 A/g, the composite electrodes exhibit good rate capability. This process opens a new window of incorporating a sufficiently small amount of SiO_x and coal tar, relative to a higher amount of graphite, to produce highly-stable SiCNW-Si/SiO_x-graphite composites. These composites can potentially replace graphite as the next generation anode material for LIB application.

Acknowledgements:

I would like to thank my supervisor, Dr. Zhongwei Chen for his assistance in the study. I would also like to thank the Department Associate Chair for graduate studies Dr. Nasser Mohieddin Abukhdeir for his timely guidance and support to ensure the completion and organization of my thesis. I am also greatly indebted to the departmental graduate coordinator Ms. Judy Caron for her constant guidance, answers to my multiple queries throughout my tenure, bringing a smile to my face during my crisis days and always offering the best solution available. Last but not the least, I have my deepest regards and respect to my departmental chair Dr Eric Croiset for having given me the opportunity to be a part of the chemical family.

A special mention must go to Dr. Boxin Zhao, Dr. Rajinder Pal, Dr V. Kodur and Dr. David Simakov, for having given the opportunity to take graduate courses under their expertise. I believe that whatever little I have inculcated in my master's study; every professor and instructor has equally contributed towards it. I would like to take this opportunity to thank the University of Waterloo, Department of Chemical Engineering and every teaching and non-teaching staff whom I have interacted with throughout my two years. In one form or another, these were the people who always made me smile, even in my worst days of struggle.

I would like to thank some of the members of the ANCEL laboratory and my colleagues including Fathy M Hassan, Kun Feng, Salah Abureden, Karthikeyan Kaliyappan, Gregory Lui, Abel Sy, Pan Xu, Altamash Jauha, Ali Ghorbani and many others. I would also like to thank my friends and well wishers for their good wishes and support throughout my study.

To spiritual guru, SHRI SHRI MOHANANANDA BRAHMACHARI MAHARAJ, Archisman is merely a soul that has been guided and projected by you on this planet to serve for the greater glory

of the Almighty. 29 August 1999 did take your mortal remains from the earth, but your soul and existence still prevails amongst us in everything we do. To Nepal Maharaj, I cannot thank you and your mother, the almighty ADYA Maa enough for including me in your divine family forever. Thanks to you and your Guru for your blessings to me and my family. To my uncle Rajatesh Banerjee, thank you for being the best support system to guide me in the correct path in life.

One may argue God is invisible. Parents are the visible God. I believe if I can make the visible God proud and happy, automatically the Almighty shall have his purpose fulfilled. To my mother Dr. Suriti Ray and father Dr. Ashok Kumar Ray. Everything I am today is because of the sacrifices both of you have made to raise me. Your unconditional love and support steers me to the path of righteousness. Needless to say, you are the best parents and the most beautiful couple in the world. To my beloved grandmother, whom I popularly called DADI, life without you post 26th July 2016 was absolutely miserable. You were my first girlfriend and my best friend. You meant everything to me. The inevitability of death did take you away from us, but your memories and your eternal presence still prevails.

Dedication:

I would like to dedicate this work to my late grandmother, Smt. Kamala Banerjee (DADI). This thesis is dedicated to her life and her life-long sacrifice she had made to raise me and my family and make me whatever I am today.

Table of Contents

List of figures

List of Abbreviations

LIBs	Lithium ion batteries
EVs	Electric vehicles
HEVs	Hybrid electric vehicles
SiCNWs	Silicon carbide nanowires
B-SICNWs	Beta-Silicon carbide nanowires
NFG	Natural flaked graphite
SEM	Scanning Electron Microscopy
TEM	Transmission Electron Microscopy
XRD	X-ray Diffraction
TGA	Thermal Gravimetric Analysis
CVD	Chemical vapour deposition
EDS	Energy dispersive X-ray spectroscopy
CV	Cyclic voltammetry
NMP	N-Methyl-2-pyrrolidone
PVDF	Polyvinylidene fluoride
Si	Silicon

SiC	Silicon carbide
NWs	Nanowires
NPs	Nanoparticles
SEI	Solid electrolyte interphase
EC	Ethylene carbonate
DEC	Diethyl carbonate
DMC	Dimethyl carbonate
FEC	Fluoroethylene Carbonate
VC	Vinylene carbonate
CMC	Carboxymethyl cellulose

1.0 Introduction

1.1 General overview

It is improbable to argue and is globally accepted that the gaseous emissions from combustion of non-renewable sources of energy, mainly fossil fuels are causing large scale air pollution across major cities. If electric vehicles (EVs) and hybrid electric vehicles (HEVs) could replace the dependency on the gasoline powered transportation system, Li-ion batteries (LIBs) could do a great extent to reduce greenhouse gas emissions when incorporated into EV.[1] LIBs are dominantly the first choice as a primary source for portable electrochemical energy storage and continue to dominate the market owing to their high energy and power density coupled with a long cycle life.[2-4] The Li-ion technology is not only dominating the consumer electronic market but is also on the verge of entering into the EV and HEV market, however, the major factor hindering it from wide market acceptance would be the limited energy density of the existing battery technology.[5] Extensive research is therefore focused on enhancing the LIB technology by reducing costs and improving the electrode performance to expand its frontier. A new era of research in Li-ion batteries has thus emerged which explores the battery electrode material and its chemistry with the intention to fabricate electrodes with a higher rate capability, higher specific capacity, longer cycle stability, and a higher coulombic efficiency. This will consequently improve the energy and power densities of LIBs, which in-turn would make it a promising candidate for the much-needed entry into the EV market.[6]

1.2 LIB- principle of operation

A typical LIB consists of a pair of lithium insertion materials alongside a separator and an electrolyte. Conventionally, the insertion material is a graphite anode, and a lithium metal oxide-

based cathode (e.g. $LiCoO_2$). With the incorporation of a lithium containing electrolyte, the lithium-ions shuttle between the positive and negative electrodes. Hence, Li-ions are continuously inserted and extracted to and from the graphite matrix. Simultaneously, electrons are extracted from one electrode and inserted into the other. The electrodes store Li-ions, while the electrolyte containing the lithium-based salt, acts as a medium for the transfer of positively charged li-ions from the anode to the cathode and vise versa via the separator. This allows for the efficient and robust storage and delivery of electrical energy when connected to a device. The most commonly used electrolyte is the lithium hexa-fluoro-phosphate ($LiPF_6$) dissolved in an alkyl carbonate-based solvent. Typically, a porous polymer-based membrane is used as the separator (typically polypropylene), which blocks the flow of electrons inside the battery, but allows the Li-ions to flow through. During the charging process, Li-ions are released by the cathode and received by the anode. While the battery is discharging and providing an electric current (when connected to a load), the anode releases Li-ions into the cathode, thereby generating a steady flow of electrons from one side to the other. Figure 1 below depicts the principle of operation of a typical LIB.

When compared to alternative rechargeable battery technologies like Nickel-Cadmium (NiCad), Nickel-Metal-Hydroxide (NiMH) and the traditional lead acid battery, LIBs have numerous advantages. Firstly, LIBs possess a higher energy density compared to any of its competing battery technologies today (100-265 Wh/kg or 250-670 Wh/L). LIB cells can deliver up to 3.6 V, which is at least three times higher than NiCad or NiMH [1]. This means that LIBs can deliver a relatively higher amount of current that is required for high-power applications. LIBs also inherently exhibit a sufficiently low self-discharge rate of around 1-2% per month and do not contain toxic elements like lead or cadmium, which makes them easier to dispose of after use as compared to the rest. Due to these advantages, LIBs have over time displaced NiCad batteries as the leader in the

portable electronic market. Currently, even leading electric cars brands like Nissan and Tesla, both use LIBs as their primary source of fuel. Recently, LIBs have also seen implemented in aerospace applications; at present NASA is conducting extensive research on LIB anode-based materials for potential application in its future space mission and projects.

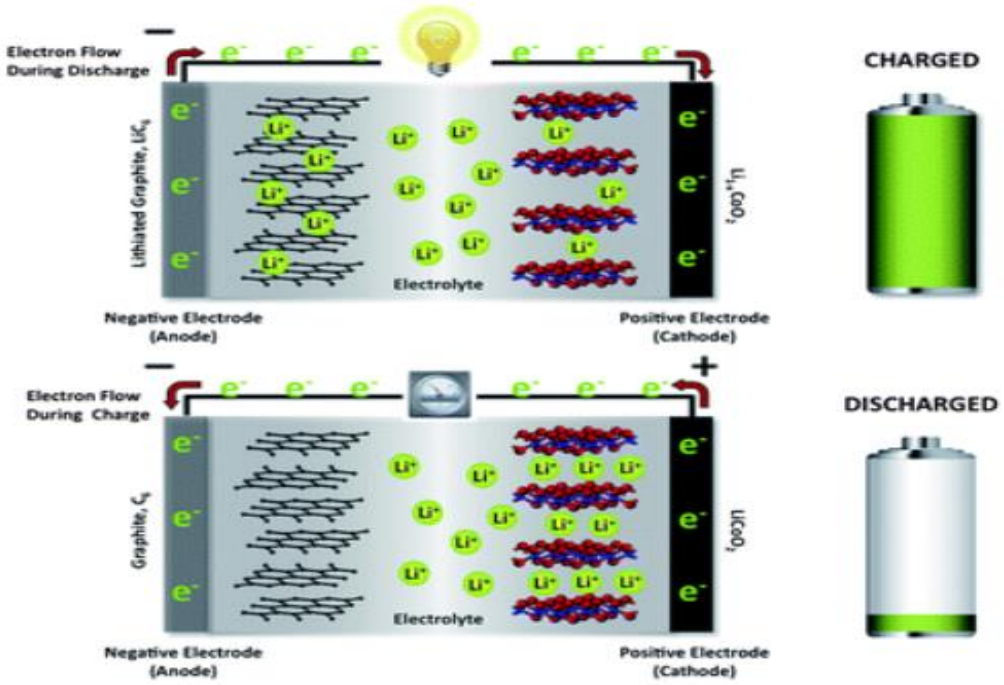

Figure 1:Schematic representation of operation of a typical LIB.

Figure 2 graphically depicts the average electrode potential versus the experimentally accessible (for the anode and the intercalation cathode materials) and theoretical (for the conversion cathodes) capacity. This figure helps us to view the various anode and cathode materials and their corresponding theoretical cell voltage, capacity, and energy density.

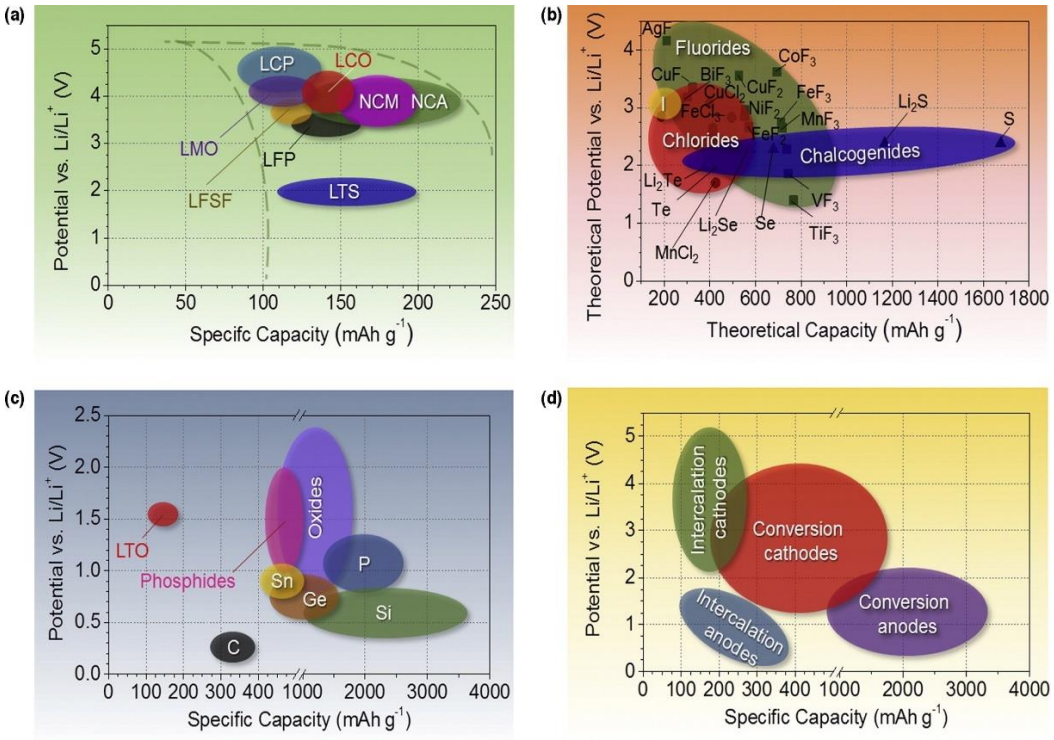

Figure 2: Approximate range of average discharge potentials and specific capacity of some of the most common (a) intercalation-type cathodes (experimental), (b) conversion-type cathodes (theoretical), (c) conversion type anodes (experimental), and (d) an overview of the average discharge potentials and specific capacities for all types of electrodes.[2] Permission from Elsevier.

Although LIBs are the primary choice source for portable electrochemical energy storage and is promising toward the EV and HEV industry, improving its performance will greatly strengthen its foundation and may enable promising new technology pertaining to energy storage. A great deal of research has therefore been carried out with the aim of modifying the LIB electrode materials. Improving the electrochemical performance of the electrode materials, while considering the total cost can ensure the advent of LIBs in the lucrative EV industry and other high-power applications.

1.3 Limitation and challenges of the current LIB technology

Although the LIB has numerous advantages as previously discussed, the LIB technology faces some shortcomings. The thermal stability of graphite as an anode material in LIBs, to this day remains a cause of genuine concern from a safety point of view. When graphite is used in a large-scale and high-voltage applications, such as that in automotive and grid applications, a fully charged LIB cell can undergo thermal runaway the moment it reaches temperatures above 160℃. This results in excess heat generation, which increases the cell temperature resulting in an uncontrollable runaway chemical reaction until the reactants are depleted. In the presence of an electrolyte, it was observed that an exothermic reaction takes place between 110 ℃ and 180℃ in lithiated carbon due to the continuous decomposition and formation of a solid electrolyte interphase (SEI).[2,7]

The primary concern is related to the aging and gradual capacity fade resulting in permanent degradation after a few years. The problem at hand is that, none of the existing electrode materials alone meet all the required performance characteristics which is comprised of:

a) High specific capacity

b) Higher energy and power density

c) Good rate performance

d) Higher operating voltage, and

e) Long cycle life.

Despite the high energy density of LIBs as compared to its competitors, they are still at least 100 times short of energy density compared to conventional gasoline, which contains 12,700 Wh/kg.

To bridge this gap, without compromising on the cost and safety is the challenge. Electrodes with a higher rate capability, higher specific capacity, longer cycle stability, and a higher coulombic efficiency will significantly improve the energy and power densities of Li-ion batteries, which in turn would make it a promising candidate for the much-needed entry into the EV market.

1.4 Motivation and thesis overview

The conventional graphite anode is a bottleneck when it comes to delivering a higher specific capacity. Although Si has a high theoretical capacity of 4200 mAh/g, Si and Si-based materials are a potential bottleneck when it comes to delivering an improved cycle life due to its inherent drawbacks. This has largely affected the implementation of the Si-based LIB technology in high end applications.

The high specific capacity of the SiO_x, coupled with the excellent long-term stability of graphite was the driving force behind fabricating novel SiCNW-Si/SiO_x-graphite based composite anode materials for LIB. These composites offer a much higher specific capacity than the graphite anode, coupled with remarkable rate capability and an excellent cycle life. The composites are also capable of accommodating the volume change of the Si particles over the repeated charge/discharge process. The SiCNWs formed in the composites, maintained the structural integrity of the composite electrodes thereby preventing the mechanical disintegration and loss of active electrode material over the repeated charge/discharge process. The thesis is comprised of six distinct sections:

(1) A general introduction, which introduces the readers to an overview of the present Li-ion technology, principle of operation of LIBs and the limitations and challenges faced by the

current technology. This section also highlights the project outline, objectives, scope and motivation.

(2) An extensive literature review on a variety of anode materials used for LIB, including those pertinent to the immediate project.

(3) A detailed discussion of the physical and electrochemical characterization techniques used in the projects.

(4) Evaluation of the performance of pristine NFG and SiO_x as anode material for LIB application (project 1).

(5) Facile synthesis of novel SiCNW-Si/SiO_x-graphite composite anode materials for LIB (project 2), and

(6) Conclusion and future work.

1.5 Thesis objectives

Generally, this thesis has the following objectives:

(a) Initially establishing a baseline which can be later improved upon. This is achieved by separately evaluating and comparing the electrochemical performance of the graphite and SiO_x based anode materials.

(b) Developing novel SiCNW-Si/SiO_x-graphite based composite anode materials with a higher specific capacity and good rate performance.

(c) Attaining a good cycle life of the composites, by effectively accommodating the volume expansion of the Si particles to prevent rapid capacity fading.

(d) Exploring a facile synthesis route and simple fabrication technique keeping in mind the cost and a possible future scaleup.

2.0 Literature review

2.1 Literature review on graphite as an anode material for LIB application

Graphite is the most widely used anode material for LIBs with a specific capacity of 372 mAh/g and an established commercial anode candidate for LIBs. Graphite-based LIBs enjoy certain advantages such as its low irreversible capacity, high 1st cycle coulombic efficiency, low discharge potential, which is close to Li metal, good specific capacity and cycle stability. However, a major issue with the graphite anode is its low specific capacity as compared to its Si counterpart.[8-10] Hence a lot of focus has recently been given to improve the performance of the graphite anode by various techniques, in order to obtain the combined advantages of enhanced cyclability, good rate capability and more importantly a higher specific capacity. Achieving this can make graphite a competitive anode candidate for the EV and HEV market, which demands a LIB with a higher specific capacity coupled with enhanced cycle life. Natarajan *et.al* for instance reduced the irreversible capacity of natural graphite and increased the first cycle coulombic efficiency from 87 % to 91.5% via CVD carried out at 800°C.[11] Yoshio *et.al* presented a simple method to change the morphology of natural graphite from originally anisotropic flaky to spherical-shaped by the "sphere-making process", and then coated carbon on the spherical graphite. The modified graphite samples exhibited a higher coulombic efficiency and higher specific capacity than the corresponding shuttle-shaped graphite sample with similar amounts of carbon coating.[12] Guopinga *et.al* later proposed a new technique to fabricate surface-modified graphite, by first milling NFG to form spherical graphite, followed by coating the spherical graphite with a layer of non-graphitic

carbon. The modified-spherical graphite was seen to exhibit superior electrochemical properties compared to the NFG and spherical graphite, having a lower irreversible capacity, higher 1st cycle coulombic efficiency and higher specific capacity.[13]

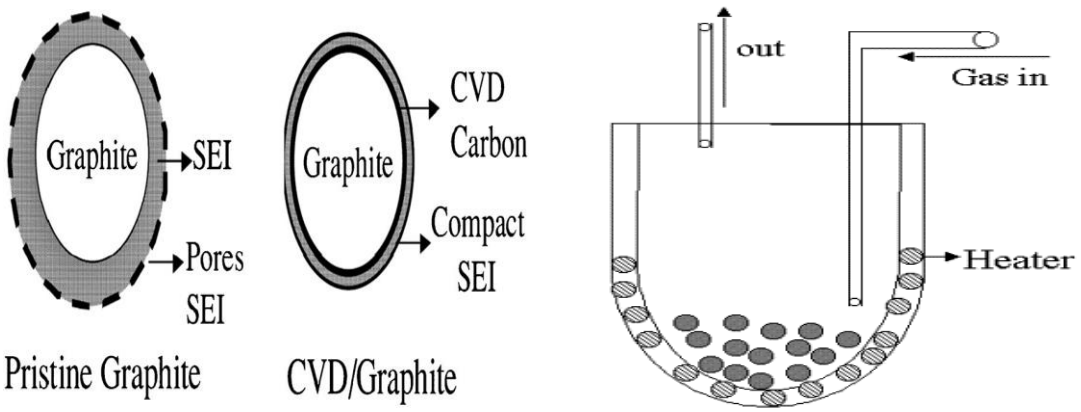

Figure 3: Schematic of the CVD process and the formation of a solid dense and stable SEI layer on graphite.[11] Permission from Elsevier.

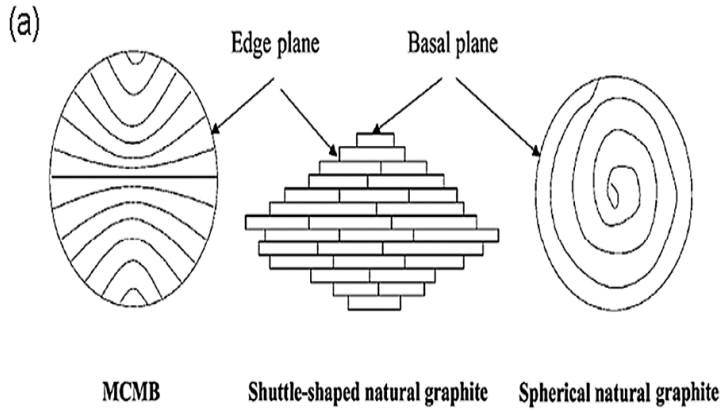

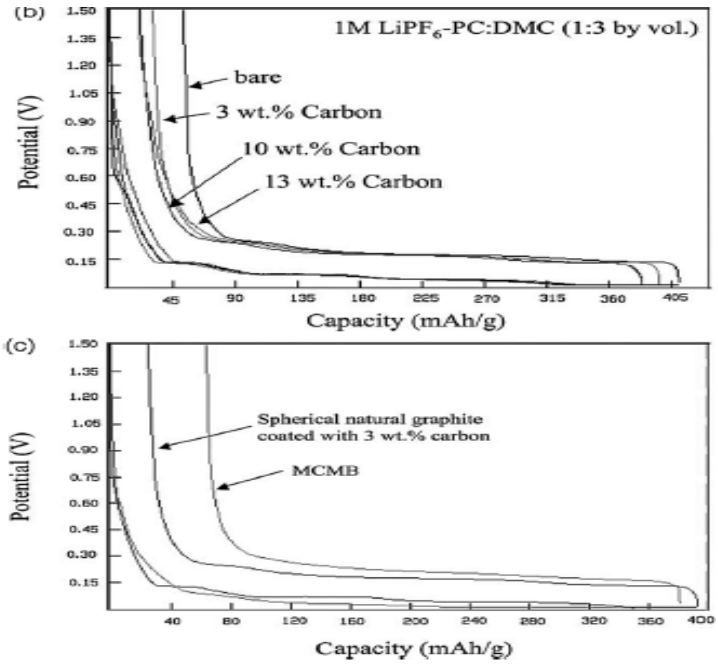

Figure 4: (a) the sphere making process (b) voltage vs capacity plot showing the increase in specific capacity with increase in carbon coating amount.[12] Permission from Wiley.

Wang *et.al* presented a novel process to fabricate sandwich-like Cr_2O_3–graphite intercalation composites via an "intercalation–transformation method", wherein Cr_2O_3 nanoparticles (NPs) were intercalated and encapsulated in the graphitic sheet layers. The composite exhibited a promising performance as anode materials for LIBs with a reversible capacity of about 480 mAh/g alongside an excellent cycling performance with over 100% capacity retention post 1000 cycles.[14] *Lee et.al* later proposed a $Li_4Ti_5O_{12}$ (LTO) coated meso-carbon micro beads (MCMB) to be used as an anode material for Li-batteries, wherein the MCMB graphite surface was uniformly coated by the LTO nanoparticles to form a core-shell structure via the sol-gel route, followed by calcination. The LTO coated MCMB were reported to exhibit an improved rate capability and cycle life, alongside superior electrochemical properties.[15]A range of composites based on graphite coupled with a second material have been seen to produce a higher capacity and enhanced electrochemical properties and have therefore been investigated as of late. Composites of Si-based

materials and graphite have also attracted widespread attention, primarily owing to the high theoretical capacity of Si as compared to other anode materials.

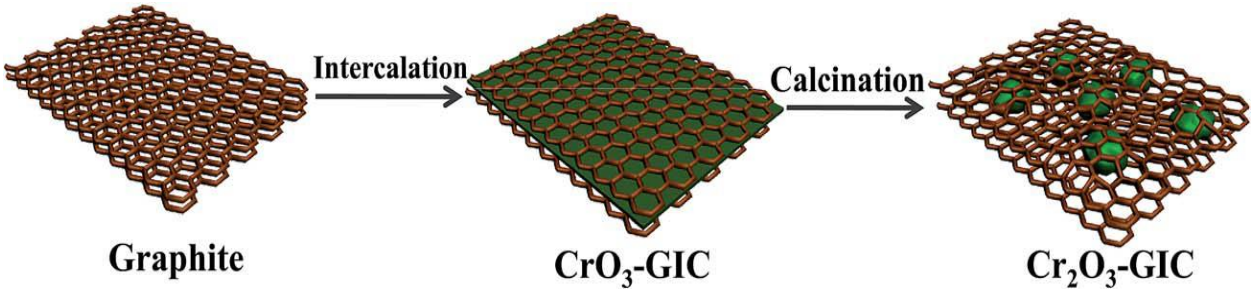

Figure 5: Schematic of the intercalation–transformation method to produce sandwich-like Cr2O3–graphite intercalation composites.[14] Permission from RSC.

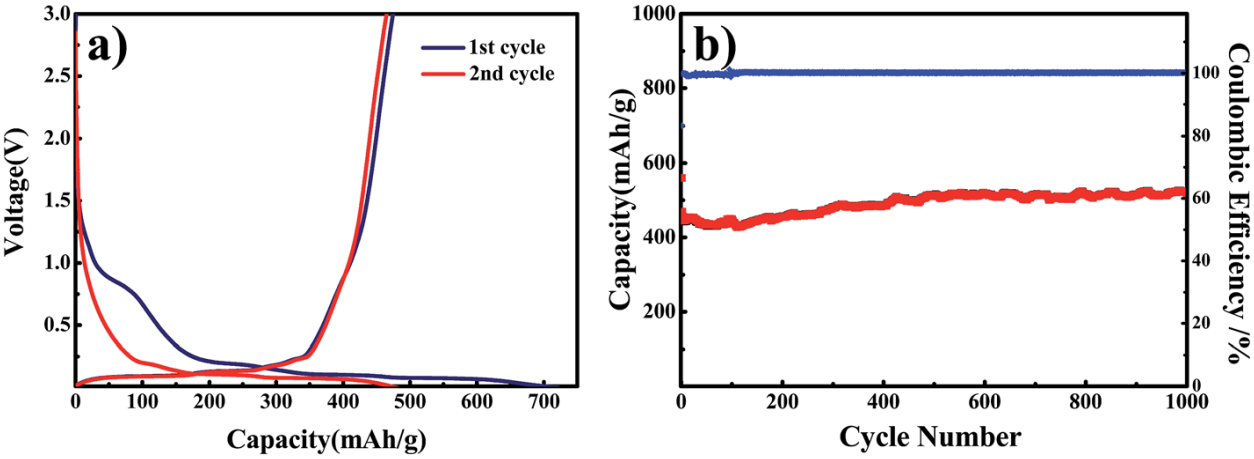

Figure 6: (a) Voltage Vs capacity profile for the first two cycles of the Cr2O3–graphite intercalation composite at 0.1 A/g (b)long-term cycle testing of the same composite at 0.1 A/g.[14] Permission from RSC.

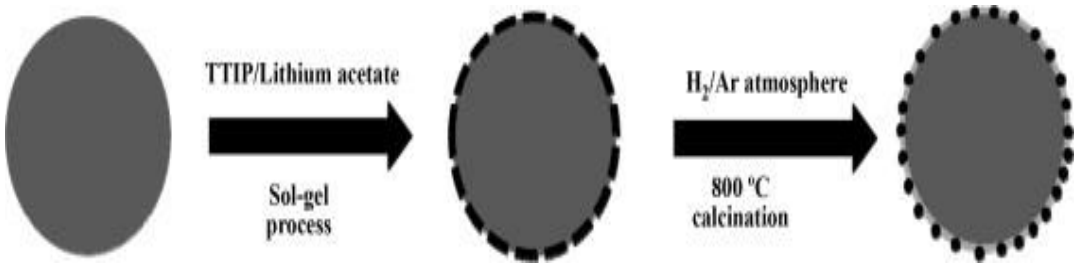

Figure 7: Schematic of the LTO-coated MCMB composite preparation method.15 Permission from Elsevier if required.

Several other techniques to modify the graphite anode have also been successfully tested. Some of these techniques include the production of mildly expanded graphite (MEG) with several defects and increased interlayer, using perchloric acid an intercalating and oxidizing agent,[16] use of an alternative binder like chitosan for improving electrochemical performance of NFG.[17]

2.2 Literature review on SiO_x based anode materials for LIB application

Graphite is the most widely used anode material for LIBs with a specific capacity of 372 mAh/g but is a bottleneck when it comes to delivering a higher specific capacity.[18-20] From the material viewpoint, Si is indeed the best choice owing to its high theoretical specific capacity of 4200 mAh/g, which is more than 10 times that of the graphite anode.[21] However, their commercial utilization in rechargeable lithium-ion batteries remains at a distance as they undergo huge changes in volume (up to 300%), during charge and discharge process. As a result of such an enormous volume change, it is very challenging to use Si alone in the cell. Hence ,extensive research is directed in finding novel, hybrid anode materials that deliver on good cycle performance, high energy and power density and long cycle life, thereby allowing it to be implemented in the EV

industry.[22-23] Recently a lot of focus has been given on the Si-based materials such as SiO and Si -alloys owing to numerous advantages such as lower volume expansion compared to its Si counterpart, relatively higher capacity (>1200 mAh/g) compared to the graphite anode and a relatively low charge-discharge potential. But the incorporation of these materials alone as an anode for LIB is far from practical reality due to its low first cycle efficiency, poor stability, low conductivity and poor cycle life.[24-25]

The SiO_x-based anode materials have over the past been modified and improved to enhance their specific capacity and cycling retention by several approaches like mechano-chemical ball-milling,[26] disproportionation reaction of SiO_x ,[27] carbon-coating technique ,[28] and the mechanical reduction of SiO_x with Li.[29]

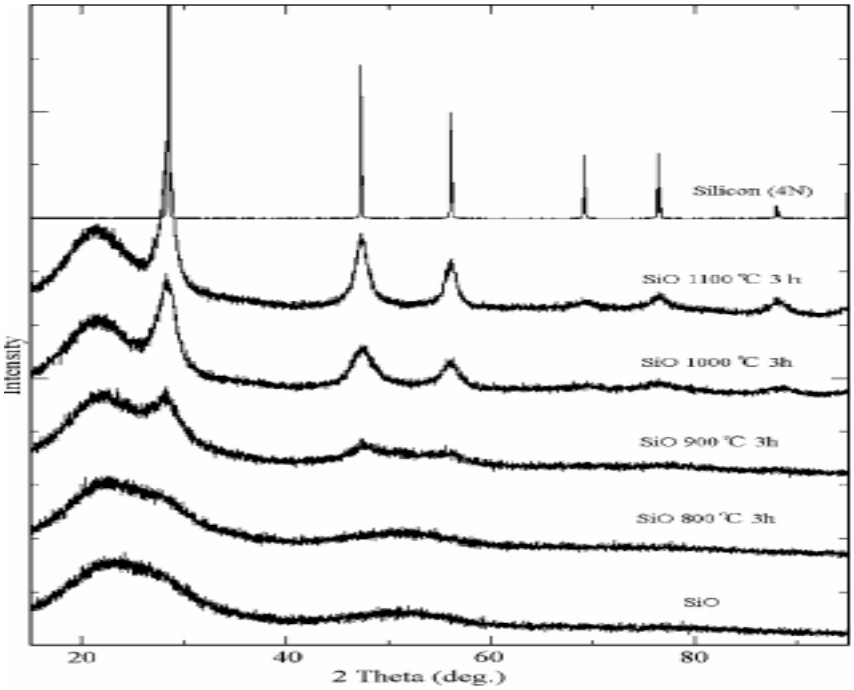

Figure 8: XRD patterns of SiO heated at various temperatures in argon flow showing the appearance of the crystalline Si peaks post annealing above 900°C.[27] Permission from ECS.

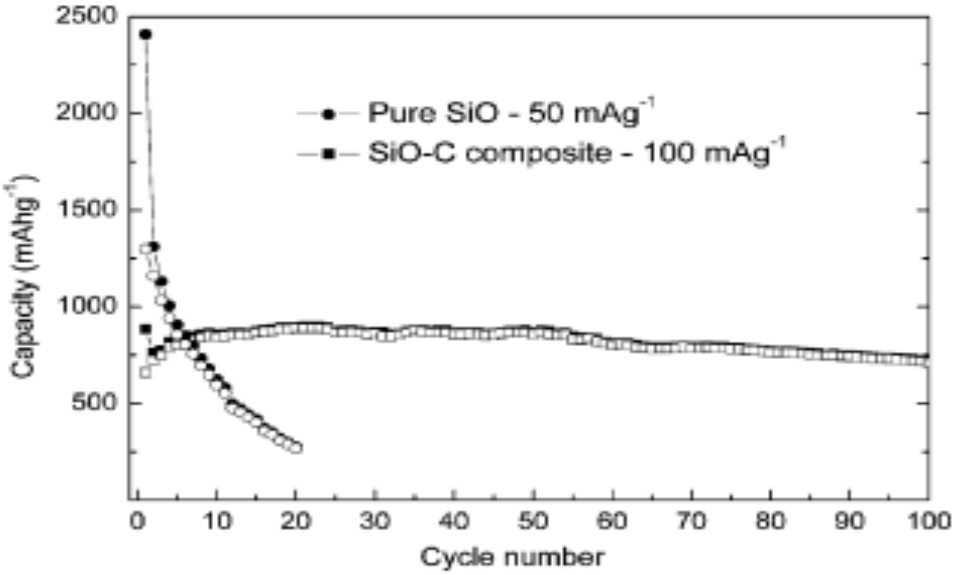

Figure 9: Enhanced cycle performance of the SiO-C composite as compared to pristine SiO post carbon treatment.[28] Permission from Elsevier.

Although the modified anode materials exhibited a significantly improved electrochemical performance, they lack a sufficient cycle life and long-term cyclability, which must be kept in mind its use for high end applications like EVs and HEVs. As discussed previously, the poor conductivity of the SiO_x-based anode materials is a primary cause of concern due to the poor contact between the particles. This directly affects the long-term cycling performance due to rapid capacity fade on the subsequent charge-discharge process. To improve and facilitate the rate capability of the SiO_x based anodes, the contact between the particles and the Li-ion from the host must be improved. To achieve this, the solid-state diffusion of lithium ions, [30] charge-transfer reactions at the electrode surface, and the corresponding Li-ion conduction in the electrolyte[31] should be considered. All this can simultaneously be achieved by enhancing the overall

conductivity of the anode. Other improvement techniques such as altering the design of the electrode materials, by nanostructuring the anode materials and synthesis of porous materials have also had promising effects on improving the rate capability and cycle life.[20,32]

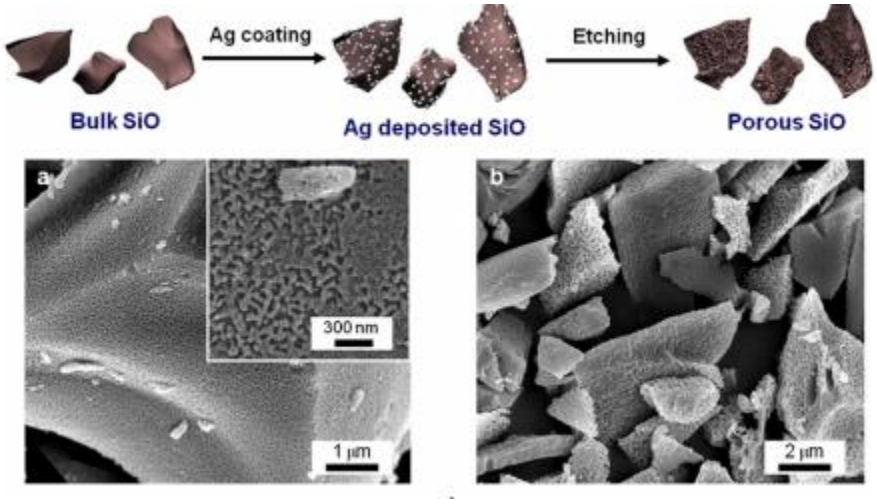

Figure 10: Enhanced cycle performance of the SiO-C composite as compared to pristine SiO post carbon treatment.[28] Permission from Elsevier.

2.3 Literature review on composites based on graphite and SiOx as anode materials for LIB

As mentioned previously, graphite is an established commercial anode with excellent stability and long cycle life. Therefore, a new trend has emerged with the aim of fabricating composite anode materials taking advantage of the stability of graphite and the high capacity of SiO_x-based materials. Compared to that of graphite alone, these hybrid materials possess a reasonably higher specific capacity coupled with good cyclability and long-term stability. Guerfi *et al.* for instance investigated the effect of various binders and carbon additives on a 1:1 by weight SiO_x-graphite

composite and found out that the addition of a reasonably small amount of carbon coated SiO_x particles (nano-particles) facilitated cycle life and higher rate capability.[33] However, their study did not mention any cycling data for the as-prepared composite. Datta *et al*. reported Si/C/PAN-C composites from extended milling of Si, graphite and polyacrylonitrile-based disordered carbon (PAN-C) led to a homogeneous dispersion of the active Si in the graphite matrix leading to a better interface adhesion between the Si and graphite particles, which in turn, resulted in a higher capacity, lower irreversible capacity loss and good capacity retention.[34] But their work was limited to merely 30 cycles. Doh *et al.* reported that the prolonged milling of graphite and SiO_x via a high-energy planetary ball-milling process, yielded composites with enhanced capacity hindering completely the formation of any side products. Again, the cycle life was limited to 30 cycles only.[35] Composites of SiOx and graphite that have been reported are therefore, either based on a high active silicon content, or limited cycle life. But, recently Qian *et al.* presented a two-step ball-milling process to fabricate $Si/SiO_x/C$ composites using commercial graphite and SiO powder, which exhibited a stable capacity of 726 mAh/g post 500 cycles at 0.1 A/g.

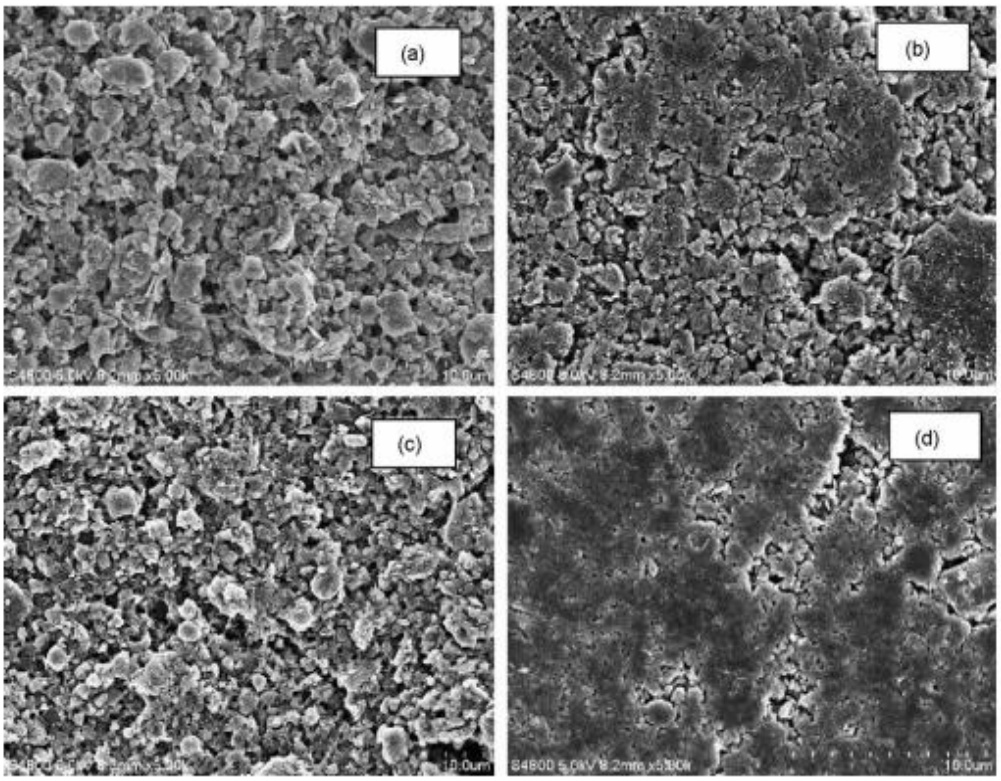

Figure 11: Enhanced cycle performance of the SiO-C composite as compared to pristine SiO post carbon treatment.[28] Permission from Elsevier.

2.4 Literature review on coal tar-based materials for LIB anode application

Coal tar is an abundant by-product from the carbonization of coal. If this abundant by-product can be recycled by incorporating it in a LIB, it would be beneficial from both the economic and environmental view point. Wang *et al.* reported a facile sintering route to prepare Si/AC nanocomposites using coal tar pitch, wherein composites of 20% Si and 80% coal tar by weight was shown to exhibit prolonged cycling with a capacity of 400.3 mAh/g alongside a high capacity retention of 71.3% after 1000 cycles.[36] Wen *et.al* fabricated multiple Si/C composites by blending Si and graphite particles in a pitch solution and pyrolyzing the mixture at elevated temperatures and reported that a simple mixture of Si and graphite could not stop the problem of rapid capacity

fading and high irreversible capacity loss. Hence, an optimum amount of graphite and pitch was required to accommodate the Si volume change and prevent the disintegration of the composite.[37] Although they showed composites of varying compositions and offered detailed explanations on their electrochemical enhancements, cycling data was again limited to only 22 cycles. Han *et al.* recently investigated the effects of varying the composition and softening point of coal tar pitches (CTPs) on the electrochemical performance of graphite-based anode materials. The CTPs with a higher softening point were found to yield a better and smoother amorphous carbon coating on the graphite surface, leading to an enhanced rate capability without necessarily compromising on the 1st cycle efficiency.[38]

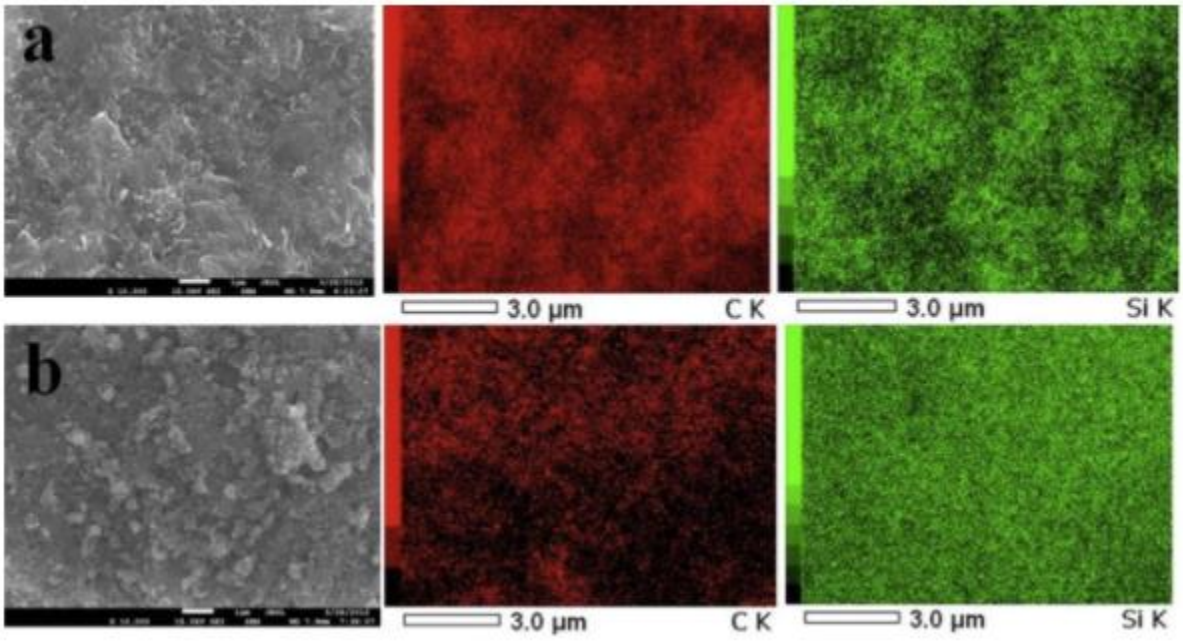

Figure 12: SEM images and corresponding elemental mappings of Coal tar pyrolyzed carbon and Silicon in (a) 0.2 Si/AC and (b) 0.5 Si/AC.[36] Permission from Elsevier.

2.5 Literature review on SiC based anode materials for LIB application

SiC has over the past been regarded as an inactive and undesired product when it comes to Si-based anode materials owing to its poor electrical conductivity and low reactivity towards Li-ions, and thereby hindering Li-ion diffusion to the Si active phase, which further causes a large irreversible capacity loss and low specific capacity.[39-40] But, Kumari *et.al* reported that cubic nano-SiC (3C polytype) prepared via a chemical vapour deposition process and commercial β-SiC powder, both when used as an anode material in a LIB, delivered high reversible capacities of around 1200 mAh/g and 668 mAh/g when cycled at C/30 rate for over 200 cycles.[41] More recently, Hu *et. al* synthesized bead-curtain shaped SiC@SiO_2 core-shell nanowires on graphite paper and tested the performance of the composite alongside bare SiC nanowires (SiCNWs) as an anode for LIB without the addition of binder and electron conductive material.[42] It was reported to possess a high specific capacity and good cycle stability, ascribing it to the unique nanowire structure which was instrumental in buffering the volume change over the repeated lithiation and de-lithiation process.[42] These findings brought to light the fact that SiC nanoparticles and SiCNWs do have a reasonable lithium insertion capacity and can be potentially incorporated as an anode material for LIB application.

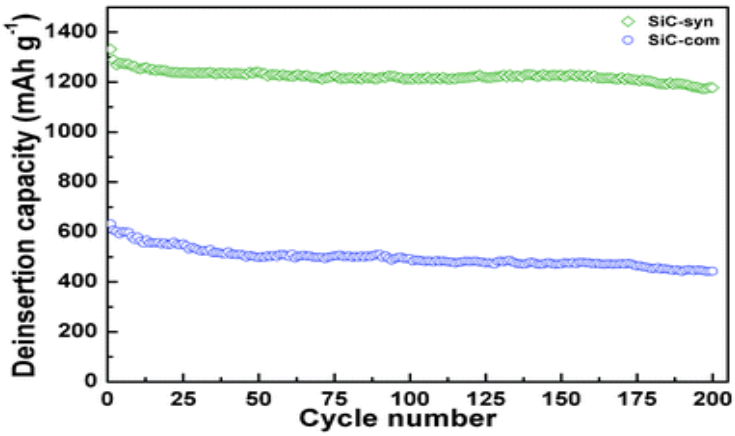

Figure 13: Cycling behavior of the as-prepared SiC and commercial SiC at C/30 rate.[41] Permission from RSC .

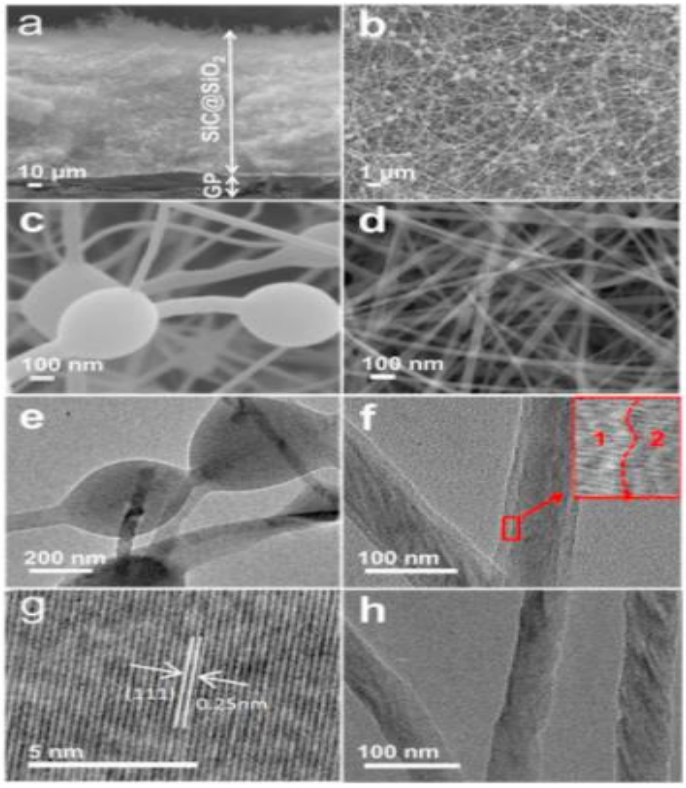

Figure 14: Morphology and microstructure observations of as-prepared materials (a-c) FESEM images of SiC@SiO2-CSNWs and (d)SiCNWs; (e-g) TEM images of SiC@SiO2-CSNWs and (h)SiCNWs.[42] Permission .

3.0 Characterization techniques

Several characterization techniques were implemented for characterizing the pristine samples and the as-prepared composite materials. The various techniques can be classified into (a) structural and physical characterization techniques and (b) electrochemical characterization techniques respectively.

The structural and physical characterization techniques used were:

- *X-ray diffraction (XRD)*
- *Scanning electron microscopy (SEM)*
- *Energy dispersive X-ray spectroscopy (EDS)*
- *Transmission electron microscopy (TEM)*
- *Thermogravimetric analysis (TGA)*

The electrochemical characterization techniques used were:

- *Galvanostatic charge-discharge test*
- *Rate capability test*
- *Long-term cycling*
- *Cyclic voltammetry test*
- *EIS*

The general working principle and application of the techniques are discussed as follows:

3.1 Physical characterization techniques

3.1.1 X-ray diffraction (XRD)

X-ray diffraction (XRD) is a powerful non-destructive technique for the characterization of powdered crystalline materials. It provides information related to the crystal structure, phase, crystal orientation, texture and other such structural parameters, such as average grain size, crystallinity, strain, and crystal defects. X-ray diffraction peaks are produced via the interference of a monochromatic beam of X-rays diffracted at various specific angles from each set of the lattice planes for a specific powdered sample. The various peak intensities are determined by the distribution of the central atoms within the lattice. The X-ray diffraction pattern is therefore a fingerprint of the periodic atomic arrangements of a given material. The ICDD (International Centre for Diffraction Data) database of X-ray diffraction patterns enables the phase identification of the sample as compared to a database of a variety of enlisted crystalline samples.

The X-ray incident beams on a crystalline solid are consequently diffracted by the crystallographic planes, following the Bragg's law. It is a simple model explaining the conditions required for diffraction, and is given as:

$2d\sin\theta = n\lambda$ ……..…**Equation1: Bragg's law**

Here, d is the spacing between the two planes hkl, n is an integer and λ is the wavelength. For parallel planes of atoms, with a spacing d_{hkl} between the planes, constructive interference occurs only when Bragg's law is satisfied. Figure 15 below, explains the Bragg's law. Two in-phase incident waves are deflected by two crystal planes (*Z and* Z_1). The diffracted waves will be in phase when the Bragg's Law is satisfied. In order to keep these beams in phase, their path difference (SQ + QT) has to equal one or multiple X-ray wavelengths (nλ) i.e. SQ + QT = nλ or

SQ + QT = 2PQ sin θ = 2d sin θ = nλ. Hence the path difference depends on the incident angle (θ) and spacing between the parallel crystal planes (*d*).

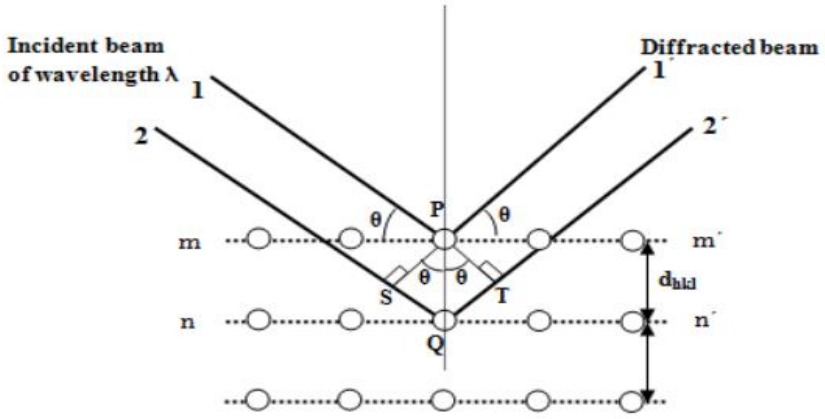

Figure 15: Figure explaining Bragg's law of diffraction

The instrument used to conduct the XRD analysis is called an X-ray diffractometer. As shown in Figure 16, a typical diffractometer usually consists of an X-ray source, a goniometer, which is the platform that holds and moves the sample, a sample holder and a detector to count the number of X Rays scattered by the sample. In the diffractometer, an X-ray beam of a single wavelength is used to examine the various specimens. By continuously changing the incident angle of the X-ray beam, a spectrum of diffraction intensity versus the angle between incident and diffraction beam is recorded. The X-ray radiation generated by the X-ray tube passes through the slits which collimate the X-ray beam. Then, the X-ray beam passing through the slits strikes the specimen and are diffracted by the specimen and form a convergent beam at the receiving slits before they enter a detector. The diffracted X-ray beam passes through a monochromatic filter to suppress

wavelengths other than K_a radiation and decrease any background radiation, before being received by the detector. The K_a radiation is generated by bombarding of target surface by the accelerated electrons. Most commonly a Cu target is used generating K_a wave length of around 0.154 nm. The relative movements among the X-ray tube, specimen and the detector ensure the recording of diffraction intensity in a range of 2θ.

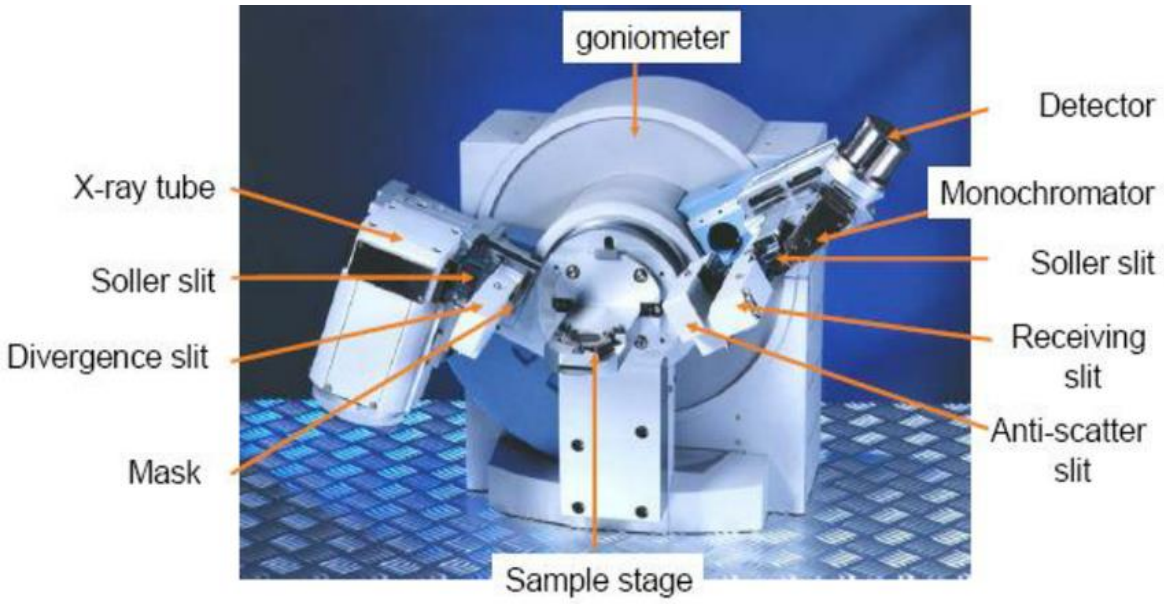

.

Figure 16: A typical X-ray diffractometer showing all its working components.

In this thesis, the various powdered samples will be analyzed, and the corresponding X-ray powder diffraction patterns shall be obtained using a MiniFlex 600 Rigaku unit, to determine the crystalline peaks of the various samples using Cu Kα radiation at 35 kV. The primary purpose in using an XRD characterization technique is to identify the various characteristic peaks ascribing to Si, graphite and β-SiCNWs in the pristine and in the as-prepared composite materials.

3.1.2 Scanning electron microscopy (SEM)

Scanning electron microscopy (SEM) is a very useful technique to detect a sample's surface topology and surface composition. A SEM represents the visual observation of an area of interest in a completely different way from what is visible to the naked eye or even normal optical microscopy. SEM images show the simple contrasts between various materials of interest and thus are capable of instantly providing information about the area of interest being inspected. The scanning electron microscope (SEM) uses a highly focused beam of high-energy electrons to generate a variety of signals at the surface of solid specimens. These signals reveal information regarding the sample including external morphology (texture), chemical composition, and crystalline structure and orientation of materials that constitute the sample. The data is collected over a selected target area of the surface of the sample, and a 2-dimensional image is generated that displays spatial variations in the properties of interest. Areas ranging from approximately 1 cm up to several microns (in width) can be imaged by using a SEM (magnification ranging from 20X to approximately 30,000X, spatial resolution of 50 to 100 nm).

The SEM works in the simple principle, wherein a beam of electrons is focused on a target area of the sample, resulting in the transfer of energy to the area. These bombarding electrons, also referred to as primary electrons, dislodge the electrons from the specimen itself. The dislodged electrons are known as the secondary electrons. These electrons are then collected by a positively biased grid and then translated in the form of a signal. To produce the SEM image, the electron beam is swept across the area under inspection, producing several such signals. These signals are then amplified and analyzed by translating them into images ascribing to the topography being

inspected. Finally, the image is projected and shown on a CRT (cathode ray tube). Figure 17 below, shows a typical SEM system illustrating the various working parts.

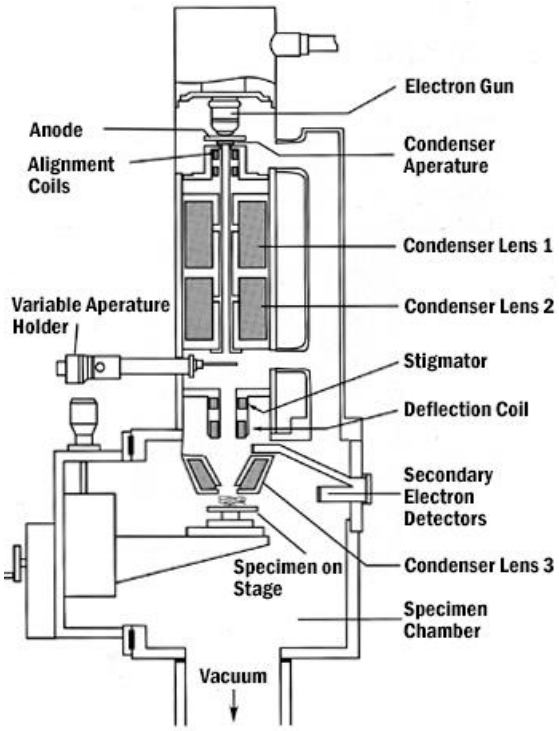

Figure 17: Schematic of a typical SEM system

SEM characterization will be used to characterize the surface morphology of the various pristine and as-prepared composite materials and provide visual confirmation of their constituent components. The corresponding particle sizes and uniform distribution of the components can also be observed. A ZEISS ULTRA PLUS, SEM device was used for the SEM characterization.

3.1.3 Energy dispersive X-ray spectroscopy (EDS)

A SEM may also be equipped with an EDS analysis system to enable it to perform compositional analysis on the selected specimen. It can also be used to find possible contaminants, as well as estimate their relative concentrations on the surface of the specimen. This approach is especially useful in the qualitative and semi-quantitative analysis of the chemical compositions, crystalline structure and crystal orientations of the material of interest. It is possible to obtain spot, line, and area maps of elements from the corresponding SEM image of the target section of the sample under investigation. These maps may be colour coded with several elemental maps superimposed. The elemental mapping images can also be superimposed on the secondary electron or backscattered electron images to obtain a comparative representation of the various elements on the specimen.

The EDS elemental mapping technique will be used in this thesis mainly to map carbon, oxygen and silicon for the SEM image of the as-prepared SiCNW-Si/SiO_x-graphite composites and to obtain the elemental overlay by superimposing the individual mapping images of carbon, oxygen and silicon. The overall mapping will be used to confirm the uniform distribution of the Si/SiO_x particles in the composite structure.

3.1.4 Transmission electron microscopy (TEM)

The transmission electron microscopy (TEM) technique, as the name suggests, makes use of the transmitted electrons (the electrons which are passing through the sample before they are collected). As a result, TEM offers invaluable information on the inner structure of the sample, such as crystal structure, morphology and stress related information, while SEM provides information limited to the sample's surface and composition. One of the most prominent difference between the two methods is the optimal spatial resolution that they can achieve. SEM resolution is limited to ~0.5 nm, while TEM images with spatial resolution of even less than 50 pm have been reported. Also, they differ in the way they are operated. SEMs usually use acceleration voltages up to 30 kV, while TEM users can set it in the range of 60 – 300kV.The magnifications that TEMs offer are also much higher compared to SEMs as the TEM allows the user to magnify their samples by more than 50 million times, while for the SEM this is limited up to 1-2 million times. In addition, the way images are created are different in the two systems. Figure 18 shows a typical schematic of a TEM system. In TEMs, samples are positioned at the bottom of the electron column and the scattered electrons (back-scattered or secondary) are captured by electron detectors. Photomultipliers are then used to convert this signal into a voltage signal, which is amplified and gives rise to the image on a PC screen. In terms of similarity and working principle, for both techniques, electrons are used in order to acquire images of samples and their main components which comprise of an electron source, a series of electromagnetic and electrostatic lenses to control the shape and trajectory of the electron beam and electron apertures.

TEM characterization will mainly be used in this thesis to point out the distinct presence of the thread like SiCNWs and micro-nano sized Si/SiO_x clusters in the as-prepared SiCNW-Si/SiO_x-graphite composite materials, in order to provide a better insight and understanding of the unique

architecture of the as-prepared composites. The TEM technique shall also be used to determine the particle size of the nanowire and Si particles in the composite structure. A Phillips CM 12 TEM device was used and the various samples were prepared by dispersing very small quantities of the powdered sample in pure ethanol, followed by drop-casting in the TEM grid.

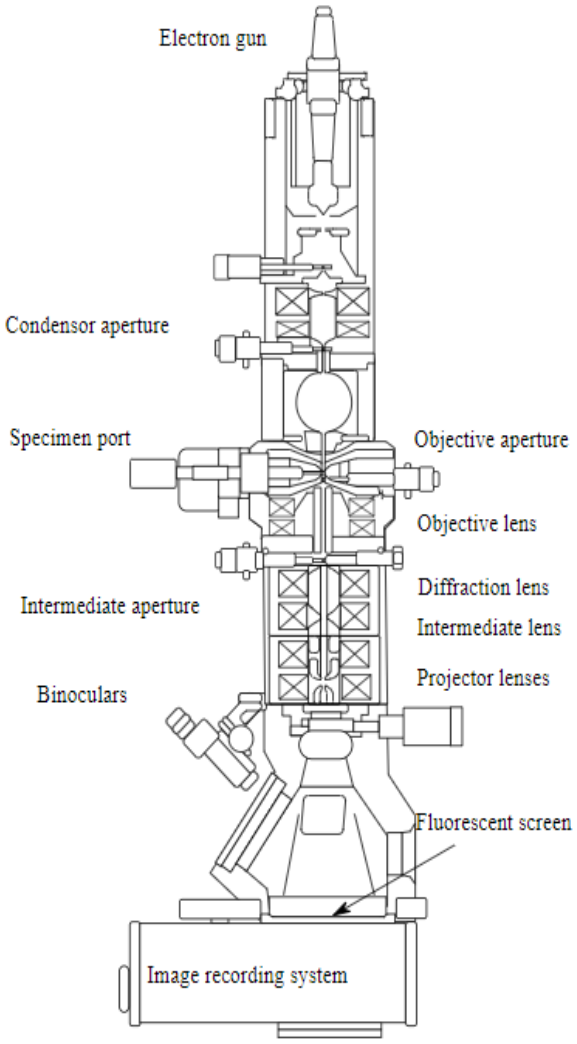

Figure 18: Schematic of a typical TEM system

3.1.5 Thermogravimetric analysis (TGA)

Thermogravimetric analysis (TGA) is used to measure the amount and rate of change in weight of a material with respect to a certain temperature and time in a specific atmosphere or condition. As shown in Figure 19, a typical TGA apparatus contains a precision balance, an auto sampler pan, and a programmable furnace with a thermocouple. The TGA provides a wide array of information of a sample like its melting point, boiling point, combustion temperature, and composition of its constituents. The furnace, which is made of quartz, can raise the temperature to as high as 1000℃. The autosampler helps to load the samples in the microbalance and the thermocouple sits right above the sample to be tested.

In this thesis, TGA thermal analysis will be performed on the as-prepared composites post milling and annealing at 1000℃, to find the relative percentage of SiCNWs and free silicon formed in the composites post heat treatment, and to find the exact amount of graphite that is lost owing to oxidation of the sample in air. A TGA Q500 apparatus in air was used in the range 80℃ to 900℃ at a ramping rate of 10℃ /min.

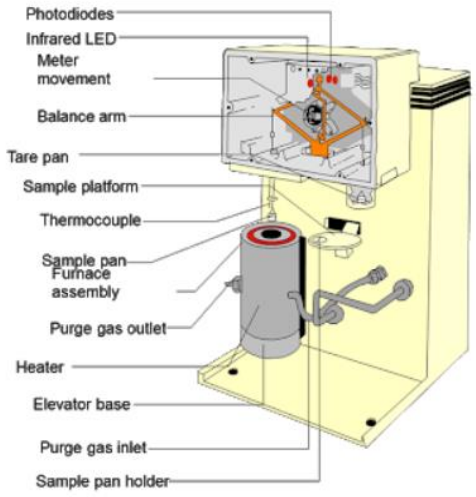

Figure 19: Schematic of a typical Q50 TGA system

3.2 Electrochemical characterization techniques

In order to evaluate the electrochemical performance of the different materials, they were tested as an anode material for a LIB by fabricating CR2032 type lithium ion coin cells. The electrode composition was varied depending on the material. For the pristine graphite-based electrodes, an electrode composition of 8:1:1 *i.e.* 80% active material,10% super-P and 10% polyvinylidene fluoride (PVDF) binder was used. For the SiO_x based cells and the composite project, a similar ratio was used, but the binder used was carboxymethyl cellulose (CMC) instead of PVDF.

For the slurry preparation, the active material powder was mixed with super-P as the conductive additive and the characteristic binder (PVDF for graphite-based cells and CMC for the SiO_x and composite cells) in the weight ratio of 8:1:1 and dissolved evenly in a suitable solvent. The solvent used for the pristine graphite project was N-Methyl-2-pyrrolidone (NMP) and that for the SiOx and composite based cells was DI water. The solvent and the entire contents were rotated at a speed of 400 rpm in a planetary centrifugal mixer for 10 min, followed by another 10 min of ultrasonication in a DI water filled sonicator for a thorough dispersion and distribution of the slurry in the solvent. This process was repeated 4 times, and then the slurry was cast on a clean Cu foil using a doctor blade and dried overnight in a vacuum oven maintained at 80℃. The Cu foil was thoroughly cleaned and rinsed with ethanol before the casting process. The dried sheets were subsequently punched in a precision disc cutter to obtain circular working electrodes and assembled into several coin-type half-cells (2032-R), with pure lithium metal foil as the counter electrode and a polypropylene (PP) based membrane as a separator, in an argon filled glovebox. The electrolyte used was 1 M LiPF6 in ethylene carbonate (EC)/dimethyl carbonate (DMC) (3:7 v/v). Fig.20 below, illustrates the various components of a typical CR-2032 type coin cell used throughout the project.

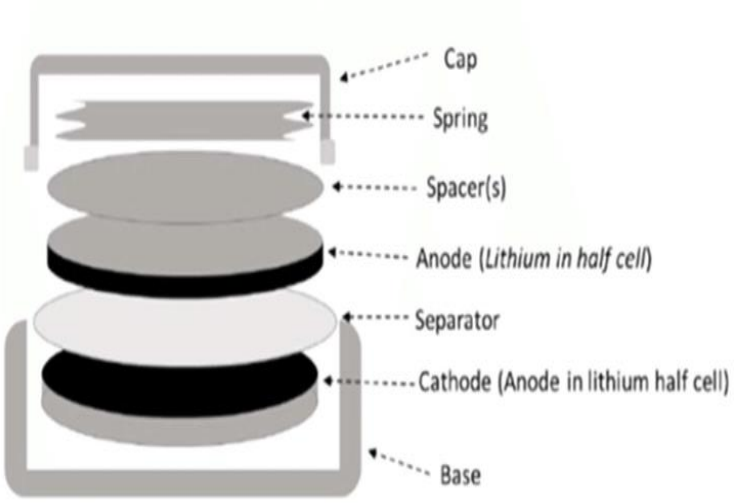

Figure 20: Schematic showing the components of the fabricated coin-type half cells.

3.2.1 Galvanostatic measurements

During the galvanostatic cycling of a battery, the charge and discharge currents are expressed in the form of a C-rate. This C is calculated from the corresponding capacity of the active material of the battery in use. The C-rate is simply a measure of the rate at which the battery in use is charged /discharged relative to its maximum theoretical capacity. Since the capacity is usually expressed in Ampere per hour, the current necessary to charge or discharge a battery can easily be calculated. By calculating the current, a constant current charge and discharge technique was applied which was used to obtain the cycling performance and the charge-discharge voltage profile data process. Hence the long-term performance of the battery was evaluated for a required number of charge-discharge cycles. The rate capability data was also obtained when different currents at different C rates were calculated and applied in the charge-discharge tests.

3.2.2 Cyclic voltammetry (CV)

Cyclic voltammetry (CV) is a powerful and popular electrochemical tool that is commonly employed to investigate the reduction and oxidation processes in an electrode. It can be used to determine the characteristic peak of the electrode reactions. The technique involves the measurement of the current that develops in an electrochemical cell under conditions where the voltage is in excess of that estimated from the Nernst equation. CV is performed by cycling the potential of a working electrode and measuring the resulting current. The voltage of the working electrode is measured against a reference electrode which is maintained at a constant potential. As a result, the resulting applied potential produces an excitation signal at a given scan rate. CV can therefore be used to quantitatively provide information on the electrochemical processes taking place under various conditions such as identifying the presence of intermediates in the oxidation-reduction process and establishing the reversibility of a reaction or process.

In this work, cyclic voltammetry (CV) measurements were performed between 0.01-1.5 V using a Gamry IFC-5000 workstation at a scan rate of 0.05 mV/s. The CV is used mainly to determine the characteristic anodic and cathodic peaks of Si and graphite as a result of their lithiation and delithiation reactions.

4.0 Evaluation of the performance of pristine NFG and SiO_x as anode material for LIB

4.1 Introduction and purpose of study

Graphite is the most widely used anode material for LIB application with a specific capacity of 372 mAh/g but is a bottleneck when it comes to delivering a higher specific capacity.[43-45] From the material viewpoint, Si is indeed the best choice owing to its high theoretical specific capacity of 4200 mAh/g, which is more than 10 times that of the graphite anode.[46] However, their practical implementation in rechargeable lithium-ion batteries is still far from reality as they undergo huge changes in volume (up to 300%), during charge and discharge process. As a result of such an enormous volume change, it is very challenging to use Si alone in the cell.[47-48] Recently a lot of focus has been given on the Si-based materials like SiO and Si alloys owing to advantages like lower volume expansion compared to its Si counterpart, relatively higher capacity (>1200 mAh/g) compared to the graphite anode and a relatively low charge-discharge potential.

The purpose of this project is to establish a baseline which can be later improved upon. Before a composite material can be synthesized, it is of prime importance to establish the baseline performance of its constituent elements. Although this section is of a lower novelty, but it establishes some important takeaways to the next project:

(1) NFG is a good choice of baseline material with good long-term cyclability with a modest specific capacity of 295 mAh/g when cycled at a rate of 0.5C (C= 372 mA/g).

(2) SiO_x yields a relatively high initial capacity which is almost 5 times that of its graphite counterpart when cycled at 0.5 C but possesses a very poor cyclability and low first cycle coulombic efficiency mainly owing to its poor electronic conductivity.

4.2 Experimental methods

4.2.1 Morphology and Structural characterization

X-ray powder diffraction (XRD) patterns were obtained (MiniFlex 600 Rigaku) to determine the crystalline peaks of the various samples using Cu Kα radiation at 35 kV. The morphology of the various samples was investigated using a scanning electron microscope (SEM) (ZEISS ULTRA PLUS, UK).

4.2.2 Electrochemical characterization

For the slurry preparation for the NFG electrodes, the NFG powder (325 mesh, Sigma Aldrich) was mixed with carbon black/super P (Alfa Aesar) as the conductive additive and poly (vinylidene fluoride) (Sigma Aldrich) in the weight ratio of 8:1:1 and dissolved evenly in N-methyl-2-pyrrolidone (NMP) solvent. For the SiO_x based electrodes, the commercially available amorphous SiO_x powder (Sino Surplus, 325 mesh) was mixed with carbon black/super P (Alfa Aesar) as the conductive additive and sodium carboxymethyl cellulose (CMC) as the binder (Aldrich) in the weight ratio of 8:1:1 and dissolved evenly in water as solvent.

The NFG and SiO_x based slurry contents were then separately rotated at a speed of 400 rpm in a planetary centrifugal mixer (THINKY, AR-100) for 10 min, followed by 10 min of ultrasonication in a DI water filled sonicator for even dispersion and distribution of the slurry contents in the solvent. This process was repeated 4 times and the slurry was cast on a clean Cu foil using a doctor blade and dried overnight in a vacuum oven maintained at 80°C. The Cu foil was thoroughly cleaned and rinsed with ethanol before the casting process. The dried sheets were then punched in a precision disc cutter (MTI-MSK-T-10) to obtain circular working electrodes and several batches of laboratory scale coin-type half-cells (2032-R) were fabricated using the composite electrode as

the working electrode against pure lithium metal foil (Sigma-Aldrich) as the counter electrode and Celgard 2500 membrane as a separator, in an argon filled glovebox (LAB star 10 work station, MBRAUN). The electrolyte used was 1 M LiPF6 in ethylene carbonate (EC)/dimethyl carbonate (DMC) (3:7 v/v). The coin-type half-cells were cycled in a LANHE CT2001 testing system (China) to obtain the galvanostatic charge/discharge profile and long-term cycling test. The mass loading of the graphite-based cells were 2.5–3.5 mg/cm^2 and that of the SiO_x coin cells were 1.5-2.0 mg/cm^2.

4.3 Results and discussion

The pristine samples were examined using a XRD unit to observe the crystalline peaks. Figure 21(A) corresponds to the XRD analysis of the pristine exhibited typical peaks of graphite at 26.1^o, 45^o,54.8^o, corresponding to the (002), (101) and (004) lattice orientations of graphite and the graphitic peaks between 42 ^{o} and 47 ^{o} corresponding to the rhombohedra or hexagonal phase of natural graphite.[49] Figure 21(B) depicts the XRD plot for the pristine SiO_x which exhibits an amorphous nature, consisting of amorphous Si and SiO_2 in a sub-oxide matrix. The range between 20–30° and the broad peaks are that of SiO_2 with low crystallinity and no corresponding Si peaks were observed in the sample.[50-52]

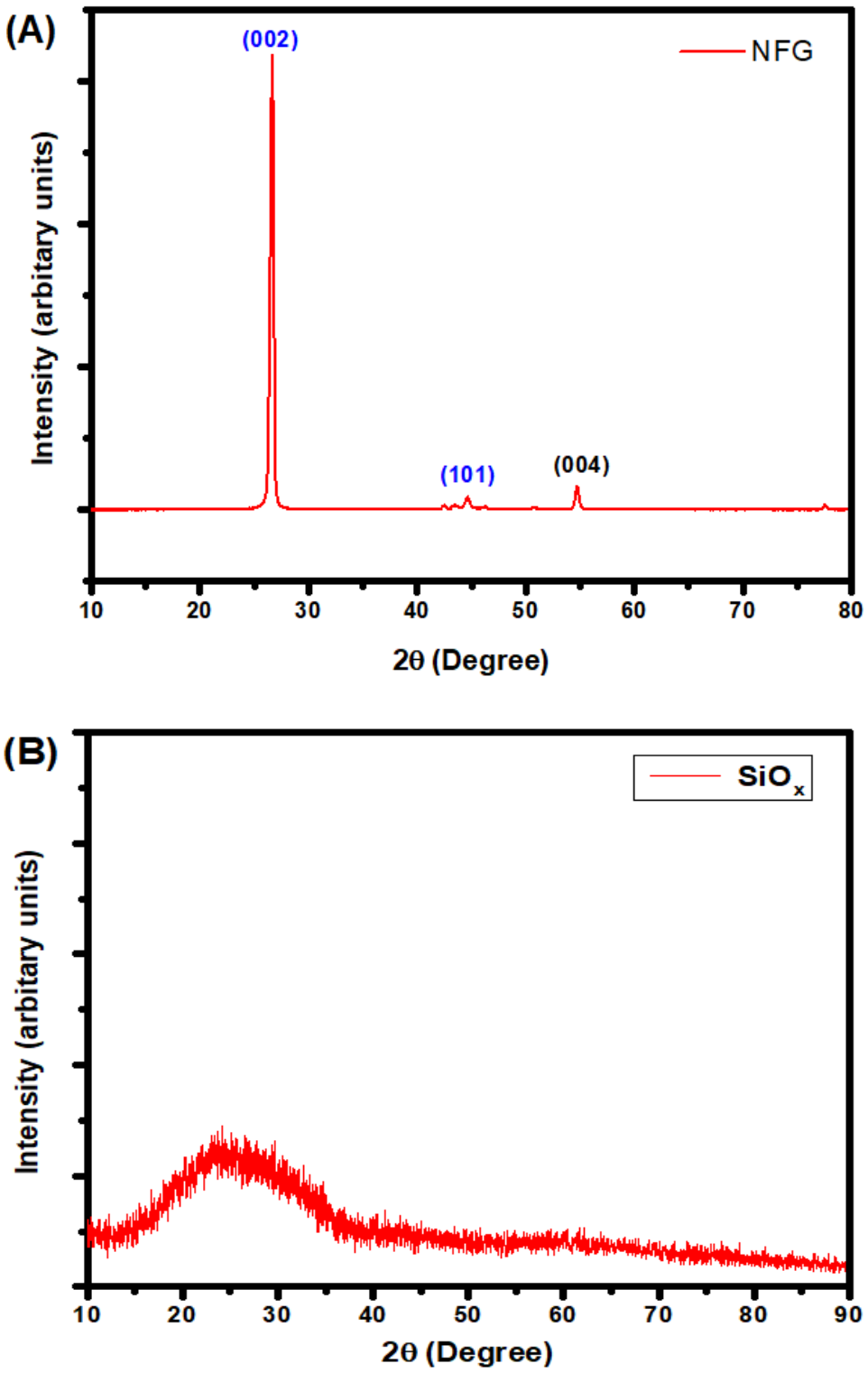

Figure 21: XRD characterization (A) NFG (B) SiOx

SEM characterization was done to investigate the morphology of the various materials including pristine NFG and SiO_x and the as-prepared composites. Figure 22(a)-(b) shows the microstructure of the pristine NFG which shows large-sized micron particles ranging between 10-20 microns with surface roughness and a typical "flake-like" appearance.[53] Figure 22(c)-(d) correspond the microstructure of the pristine SiO_x, and the particles are seen to possess a triangular-like shape spanning to several microns.

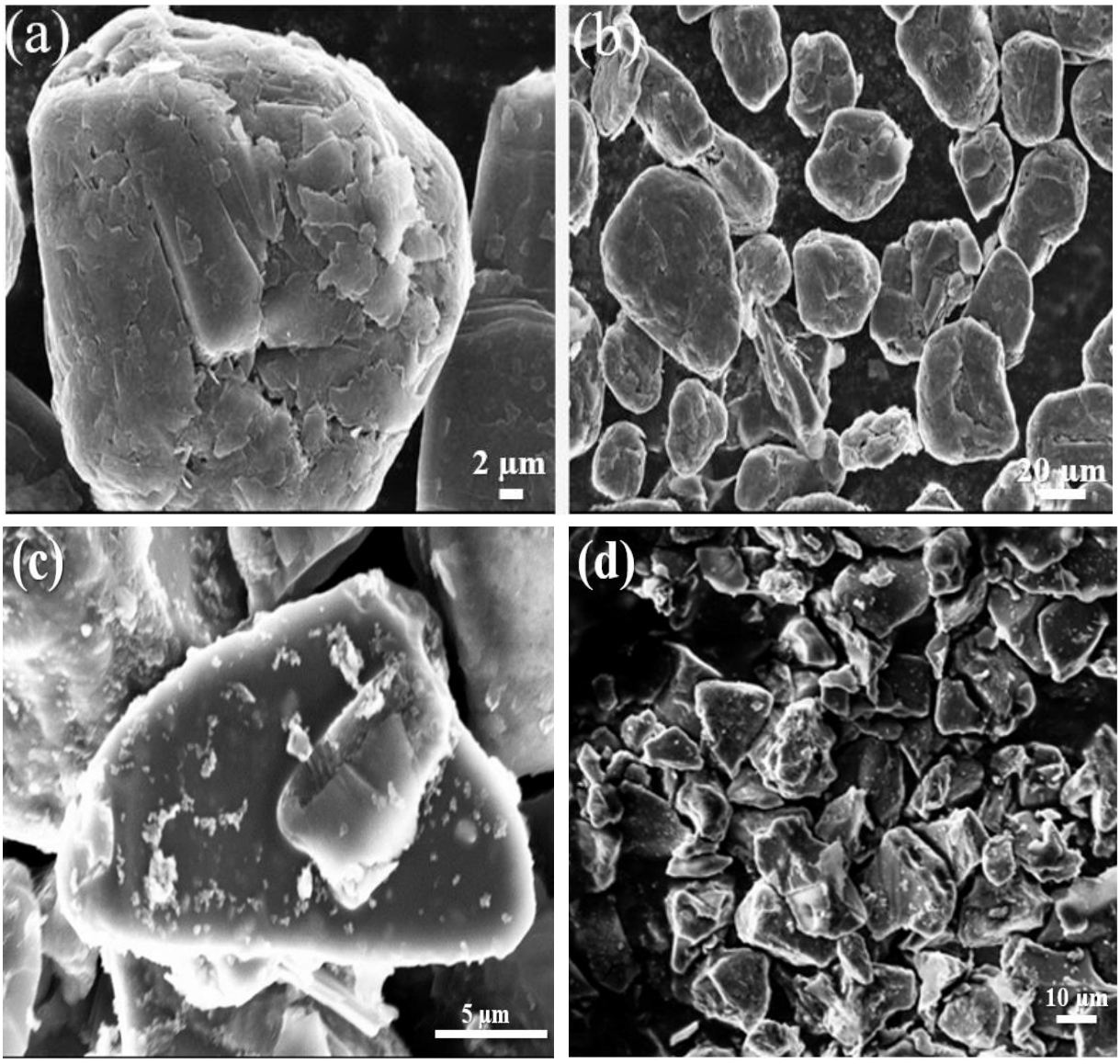

Figure 22: SEM characterization images (a)-(b) NFG (c)-(d) SiOx

The electrochemical performance of the NFG and SiO_x as an anode material for LIBs were tested by implementing it in a half coin-cell against lithium metal as the counter electrode. Figure 23(A) shows the galvanostatic charge/discharge curves for the first three cycles of the pristine NFG at a rate of 0.1C (C= 372 mA/g for graphite) within the voltage window of 0.001 V-1.5 V. The first discharge and charge capacities of the pristine NFG were found to be 438.2 mAh/g and 367.5 mAh/g respectively, yielding a high first cycle coulombic efficiency of 83.8%. The long-term cycling for the same cell is shown in Figure 23(B), wherein the cell was first subjected to a slow rate of 0.1 C for the first ten cycles, followed by subjecting it to a relatively high rate of 0.5 C from cycle 11 till the end. During the transition from 0.1 C to 0.5 C, the cell exhibited a decrease in capacity from 365 mAh/g to 295 mAh/g in the subsequent cycles, eventually yielding good capacity retention of over 80% and a stable capacity of 295 mAh/g after 210 cycles.

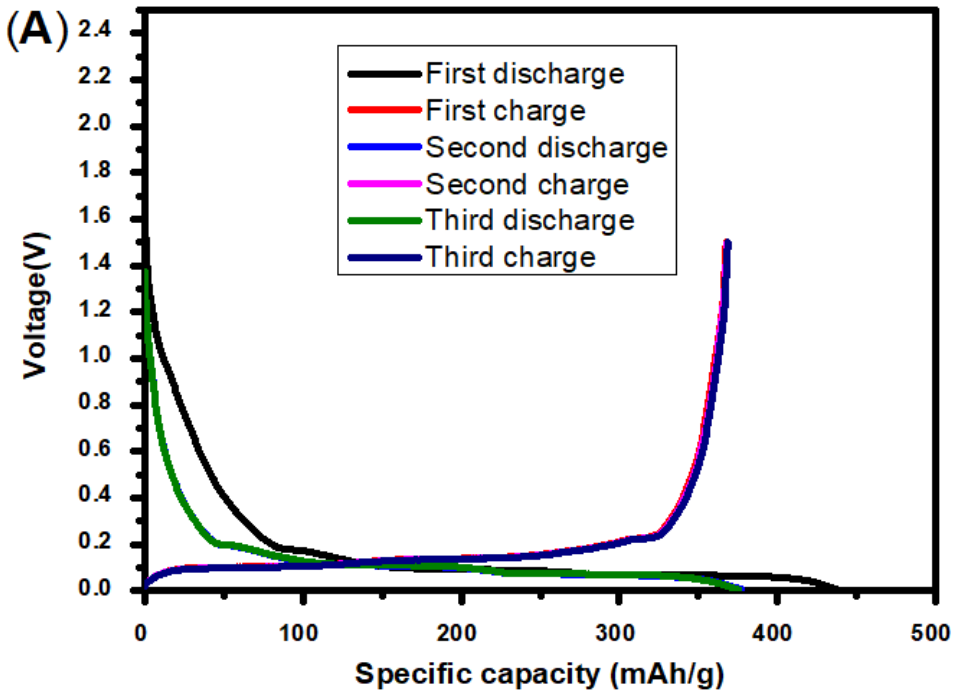

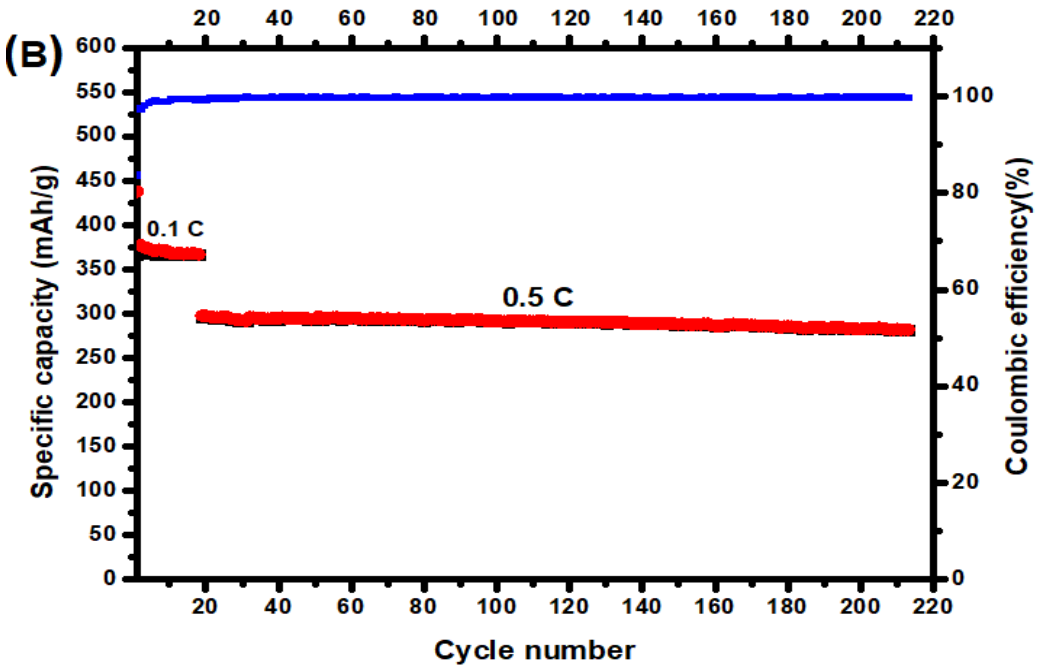

Figure 23: Electrochemical performance of NFG (A) Charge/discharge profile of NFG (B) long-term cycle performance of NFG.

A similar procedure was carried out for the pristine SiO_x half cells, wherein the cells were subjected to long-term cycling test at an initial rate of 0.1C (C= 1000 mAh/g) for the first 3 cycles, followed by 0.5 C from cycles 4 till the end. Figure 24(A) shows the charge/discharge voltage curves for the first three cycles at the rate 0.1 C and between the voltage range of 0.01V- 1.5V. The first cycle discharge and charge capacities were found to be 1557.8 mAh/g and 1057.2 mAh/g respectively, corresponding to a low first cycle coulombic efficiency of 67.8%. Figure 24(B) illustrates the long-term performance of the pristine SiO_x under similar conditions stated above. The pristine SiO_x cells showed a very poor cycling performance and lost almost 50% of its initial capacity in just 20 cycles cycled at 0.5 C. By the end of the 50^{th} cycle, the capacity of the pristine SiO_x dropped to a mere 60 mAh/g, thereby highlighting the extremely poor cyclability of the pristine SiO_x sample. Although pristine SiO_x yields a relatively high initial capacity which is almost 5 times that of its

graphite counterpart, its poor cyclability and low first cycle coulombic efficiency remains a huge concern mainly owing to its poor electronic conductivity.[24-25,54]

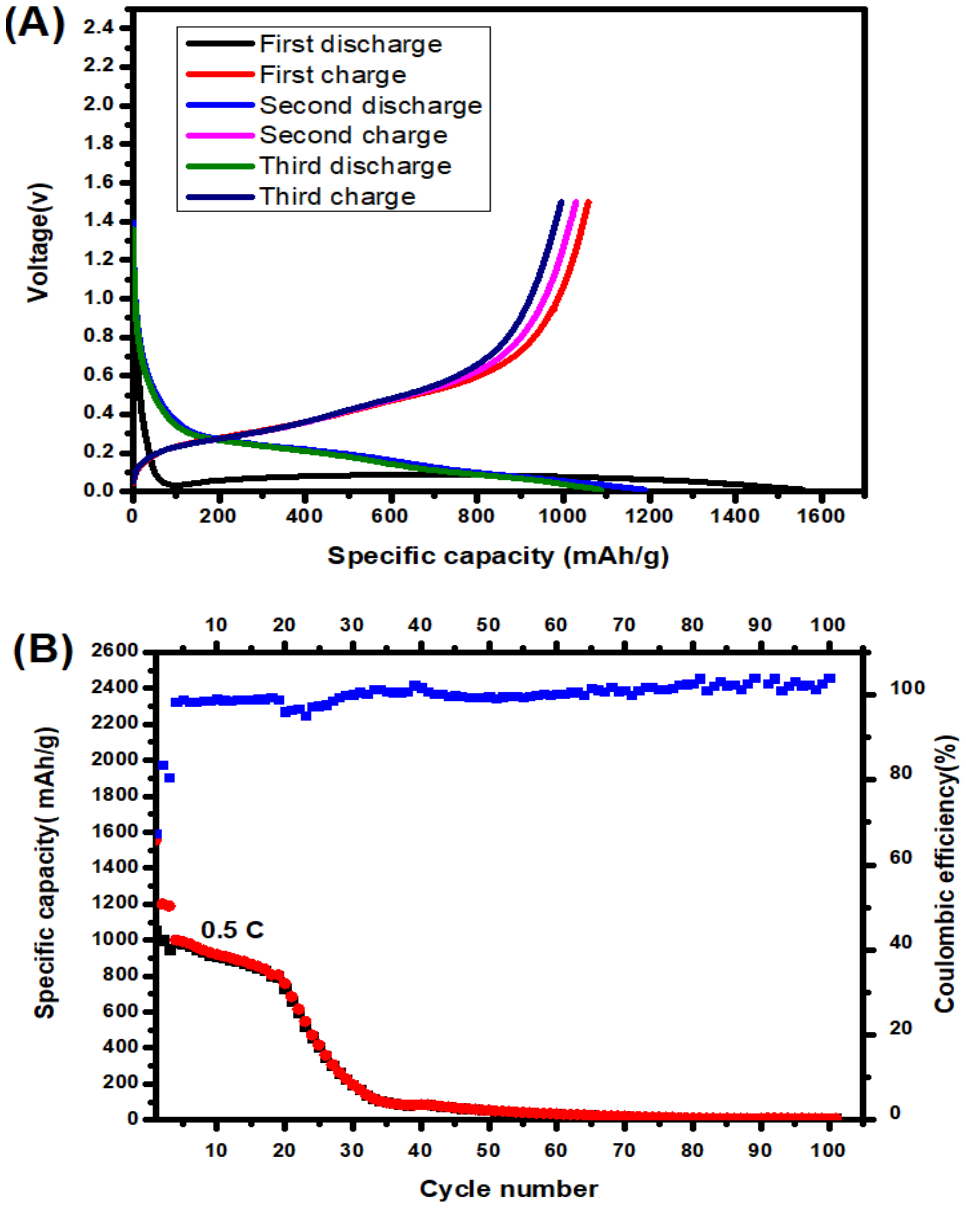

Figure 24: Electrochemical performance of SiOx (A) Charge/discharge profile of SiOx (B) long-term cycle performance of SiO

4.4 Conclusion and remarks

In summary, the electrochemical performance of the pristine NFG and SiO_x was evaluated in this project, with the aim to establish a baseline to build upon. The NFG electrodes, exhibited a good cyclability with good long-term stability and capacity retention of 80% at 0.5 C post 210 charge-discharge cycles. The SiO_x on the other hand, exhibited a very poor cyclability and lost almost 50% of its initial capacity in just 20 cycles when cycled at 0.5 C. Although SiO_x yields a relatively high initial capacity which is almost 5 times that of its graphite counterpart, its poor cyclability and low first cycle coulombic efficiency remains a huge concern mainly owing to its poor electronic conductivity.

The major takeaway from this project was that graphite is a bottleneck when it comes to delivering a higher specific capacity and SiO_x is a bottleneck when it comes to delivering an improved cycle life. On the other hand, SiO_x offers an initial specific capacity that is almost 5 times that of its graphite counterpart and graphite has a remarkable cycle life. This projects the very idea and need to create a composite anode material that delivers on both a higher specific capacity and a stable cycle life and performance, by incorporating graphite and SiO_x in the same cell. Such an anode material can potentially replace graphite as the next generation anode material for LIB and facilitate the entry of the LIB in the EV and HEV market.

5.0 Facile synthesis of novel SiCNW-Si/SiO_x-graphite composite anode materials for LIB

5.1 Introduction and purpose of study

Although graphite is the most widely used anode material for LIB application possessing a specific capacity of 372 mAh/g but is a bottleneck when it comes to delivering a higher specific capacity.[18-20] From the material perspective, Si is indeed the best choice owing to its high theoretical specific capacity of 4200 mAh/g, which is more than 10 times that of the graphite anode.[21] However, their wide utilization in rechargeable lithium-ion batteries is still far from reality as they undergo huge changes in volume (up to 300%), during charge and discharge process. As a result of such an enormous volume change, it is very challenging to use Si alone in the cell. Hence extensive research is on to find novel hybrid anode materials that deliver on good cycle performance, high energy and power density and long cycle life, thereby allowing it to be implemented in the EV industry.[22-23] Recently a lot of focus has been given on the Si-based materials like SiO and Si alloys owing to advantages like lower volume expansion compared to its Si counterpart, relatively higher capacity (>1200 mAh/g) compared to the graphite anode and a relatively low charge-discharge potential. But the incorporation of these materials alone as an anode for LIB is far from reality due to its low first cycle efficiency, poor stability, low conductivity and poor cycle life.[24-25] Graphite on the other hand is an established commercial anode with excellent stability and long cycle life. Therefore, a new trend has emerged with the aim of fabricating composite anode materials taking advantage of the stability of graphite and the high capacity of SiO_x-based materials. These hybrid materials possess a reasonably higher specific capacity compared to that of graphite coupled with good cyclability and long-term stability.

Research efforts on composites of Si and SiO_x alongside carbon are either based on a high active Si content or limited in cycle life. Coal tar is an abundant by-product of the carbonization of coal, if this abundant by-product can be recycled by incorporating it in a LIB, it would be beneficial from both the economic and environmental view point. The original goal of our study was therefore to obtain carbon coated Si/SiO_x particles by the wet ball milling SiO_x with coal tar and eventually dispersing it in a conductive graphite matrix. So, we initially mixed bulk SiO_x powder with liquid coal tar with the aim of creating a thin conductive coating around the SiO_x particles, as SiO_x is known to possess poor conductivity.[54] But on wet milling of coal tar with SiO_x, a mixture of micro-nano sized Si/SiO_x particles alongside smaller SiO_x particles covered with a thin layer of coal tar were formed. Further milling these products with graphite, followed by thermal annealing at 1000℃ leads to the formation of thread-like β-SiCNWs alongside micro-nano clusters of Si/SiO_x dispersed homogeneously in the composite matrix. This intrigued us to fabricate novel SiCNW-Si/SiOx-graphite composites by incorporating the Si/SiO_x and coal tar covered SiO_x particles formed on milling by dispersing them into the conductive graphite matrix followed by annealing at 1000℃.

The previous findings from the literature review section, also brought into light the fact that the SiC phase, which over the past years has been regarded as an inactive and undesired product when it comes to Si based anode materials, do have a reasonable lithium insertion capacity. This also intrigued us to fabricate the novel SiCNW-Si/SiOx-graphite composites. This was achieved by using a relatively low content of Si and coal tar relative to a larger portion of graphite, keeping the economic and environmental view point in mind for a possible scaleup. Composites of varying compositions were synthesized with the aim of achieving good long-term stability and increased conductivity without essentially compromising on the safety and total cost. This process not only

opens up a new window of incorporating a sufficiently small amount of SiO_x and coal tar relative to a higher amount of graphite to produce highly stable SiCNW-Si/SiO_x-graphite composites which can potentially replace graphite as the next generation anode material for lithium-ion battery application, but also presents a new facile economical route to prepare SiCNWs for a variety of applications.

5.2 Experimental methods

5.2.1 Preparation of the SiCNW-Si/SiO_x-graphite composite

Figure 25 illustrates the fabrication process of the SiCNW-Si/SiOx/graphite composites. The starting precursors for the fabrication of the composite materials were commercially available amorphous SiOx powder (Sino Surplus, 325 mesh), coal tar solution (Alfa Aesar) and NFG powder (325 mesh, Sigma Aldrich). All the chemicals reagents used were in the as-received state without any further purification. SiO_x powder was first mixed in bulk with liquid coal tar dissolved in a small amount of Tetrahydrofuran(THF) (anhydrous ,≥99.9% inhibitor-free Sigma-Aldrich) and the contents were then subjected to wet mechanical milling in a horizontal planetary ball-mill (Nanjing University Instrument Plant, China) at a rotation speed of 400 rpm for 14 h in an argon atmosphere, using stainless steel jar and balls of varying diameters (6 and 10 mm) in the ratio 3:1. The resultant milled contents were then mixed with NFG powder and a small amount of ammonium bicarbonate salt (reagent plus grade, Sigma Aldrich) and the contents were subjected to mechanical milling for a second time for around 45 min under similar milling conditions. Finally, the milled contents were carefully scraped off from the stainless steel jar and then transferred to a quartz boat and subjected to thermal annealing in a tube furnace (Thermo Scientific

Lindberg/Blue) at 1000 ℃ in an argon atmosphere by purging in high purity argon gas (99.9999 % purity, Linde Canada), where the furnace temperature was held for 3 hrs before raising the temperature to 1000 ℃ at a heating rate of 2℃/min. Subsequently, it was cooled gradually to room temperature and then collected and stored in a vial. This process was repeated by varying the weight ratio of SiO_x, coal tar, ammonium bicarbonate and NFG to prepare composites in the following weight ratios:

(1) Composite 1:(SiO_x: C: NH_4HCO_3: NFG) =10:6:4:80

(2) Composite 2:(SiO_x: C: NH_4HCO_3: NFG) =20:16:4:60

(3) Composite 3:(SiO_x: C: NH_4HCO_3: NFG) =25:11:4:60

Incorporating a two-step fabrication process of mechanical milling followed by thermal annealing, not only ensures the proper size reduction of the micro sized SiO_x particles, but also aids in the uniform distribution of the particles in the composite matrix, thereby creating a conductive route between the particles, resulting in stable composites with enhanced conductivity and superior mechanical and electrochemical properties.

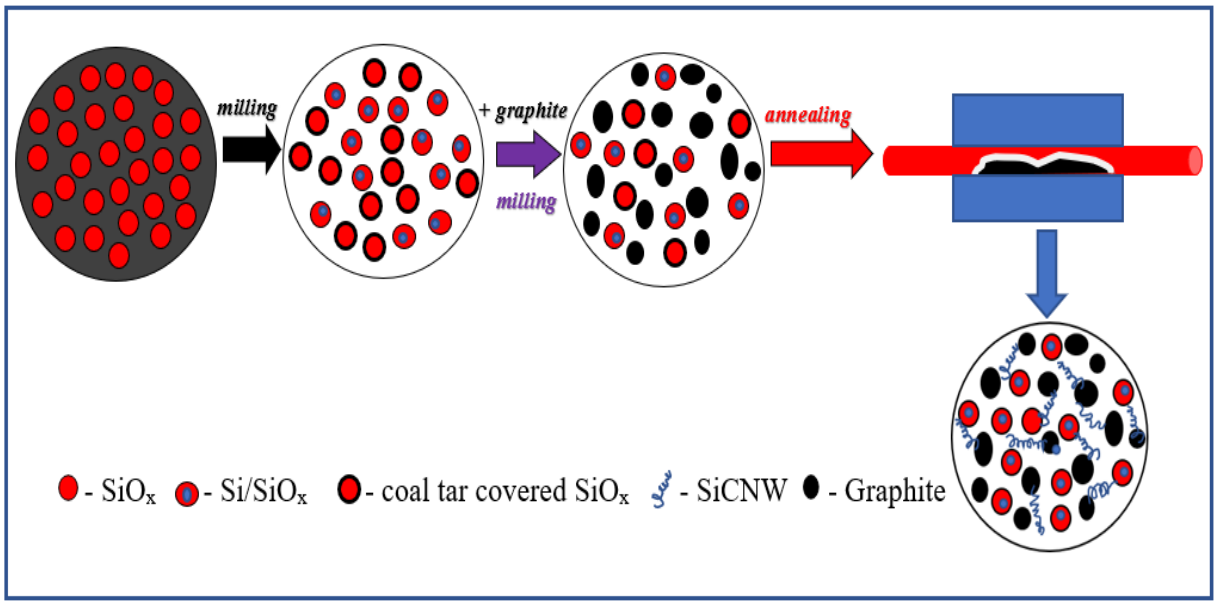

Figure 25: Schematic diagram for the preparation of the SiCNW-Si/SiOx-graphite composites.

.

5.2.2 Morphology and Structural characterization

X-ray powder diffraction (XRD) patterns were obtained (MiniFlex 600 Rigaku) to determine the crystalline peaks of the various samples using Cu Kα radiation at 35 kV. The thermogravimetric analysis (TGA) test was conducted in a TGA Q500 in air in the range 80℃ to 900℃ at a heating rate of 10℃ /min. The morphology of the various samples was investigated using a scanning electron microscope (SEM) (ZEISS ULTRA PLUS, UK). A transmission electron microscope (TEM) (Phillips CM 12, USA) was also used to find the surface morphology by dispersing very small quantities of the powdered sample in pure ethanol, followed by drop-casting in the TEM grid. The energy dispersive X-ray spectroscopy (EDS) mapping technique was also carried out using the same SEM device.

5.2.3 Electrochemical characterization

For the slurry preparation, the composite powder was mixed with carbon black/super P (Alfa Aesar) as the conductive additive and sodium carboxymethyl cellulose (CMC) as the binder (Aldrich) in the weight ratio of 8:1:1 and dissolved evenly in water as solvent and the entire contents were rotated at a speed of 400 rpm in a planetary centrifugal mixer (THINKY, AR-100) for 10 min , followed by 10 min of ultrasonication in a DI water filled sonicator for even dispersion and distribution of the slurry contents in the solvent. This process was repeated 4 times and the slurry was cast on a clean Cu foil using a doctor blade and dried overnight in a vacuum oven maintained at 80°C. The Cu foil was thoroughly cleaned and rinsed with ethanol before the casting process. The dried sheets were then punched in a precision disc cutter (MTI-MSK-T-10) to obtain circular working electrodes and several batches of laboratory scale coin-type half-cells (2032-R) were fabricated using the composite electrode as the working electrode against pure lithium metal foil (Sigma-Aldrich) as the counter electrode and Celgard 2500 membrane as a separator, in an argon filled glovebox (LABstar 10 work station, MBRAUN). The electrolyte used was 1 M LiPF6 in ethylene carbonate (EC)/dimethyl carbonate (DMC) (3:7 v/v). The coin-type half-cells were cycled in a LANHE CT2001 testing system (China) to obtain the galvanostatic charge/discharge profile, rate capability and long-term cycling test. After the cell assembly, cyclic voltammetry (CV) measurements were performed between 0.01-1.5 V using a Gamry IFC-5000 workstation with a scan rate of 0.05 mV/s. The mass loading of the composite cells was 2-3 mg/cm^2.

5.3 Results and discussion

The various samples were examined using a XRD unit to observe the crystalline peaks. Figure 26(A) illustrates a typical composite material (composite 3) after the two-step mechanical ball-milling and after thermal annealing at 1000℃ and Fig.26(B), corresponds to the XRD analysis of the as-prepared composite materials after the thermal annealing process at 1000℃. The as-prepared SiCNW-Si/SiO_x-graphite composites exhibited typical peaks of graphite at 26.1º, 45º,54.8º, corresponding to the (002), (101) and (004) lattice orientations of graphite and the graphitic peaks between 42 º and 47 º corresponding to the rhombohedra or hexagonal phase of natural graphite.[53] Distinct peaks of Si at 28.3 º, 47.2 º, 56.1 º and 88 º correspond to the (111), (220), (331) and (422) lattice orientations were observed.[55] The presence of these Si peaks is due to the disproportionation reactions of SiOx on milling to form micro-nano sized Si/SiO_x particles and on thermal annealing at 1000℃, where nano-crystalline Si particles are dispersed into the SiO_x matrix.[56-58] The peak at 43.4 º might be a possible formation of Fe_2Si which is a possible product from the milling of Si with the stainless-steel balls used in the milling process. It is known that intensive prolonged milling causes contamination with Fe from the grinding media, which in turn may act as a seed for the growth of SiC nanowires.[59] Characteristic peaks of β-SiC were observed at 35.6°, 60.0°and 71.8°, which correspond to the diffraction of β-SiC (1 1 1), (2 2 0) and (3 1 1), respectively.[41,60] Composite 1 exhibits peaks of SiC at 35.6°and 60.0° only. This can be attributed to its high graphitic content coupled with its low SiO_x content during fabrication, eventually leading to the formation of a lesser amount of SiCNWs. Figure 26(A) also highlights the fact that the β-SiC peaks are only observed after the process of thermal annealing the already milled composites, establishing the fact that the β-SiC particles are only formed during the annealing process and not during the two-step mechanical milling. Figure 26(C) depicts the XRD plot for the

pristine SiO_x and amorphous carbon derived from thermal annealing of the as-received coal tar at 1000℃. The pristine SiO_x exhibits an amorphous nature, consisting of amorphous Si and SiO_2 in a sub-oxide matrix. The range between 20–30° and the broad peaks are that of SiO_2 with low crystallinity and no corresponding Si peaks were observed in the sample.[61-63] The amorphous carbon derived from annealing coal tar, shows a set of broad peaks at around 24°and 43°corresponding to the (002) and (100) crystallographic planes of low graphitized amorphous carbon.[64]

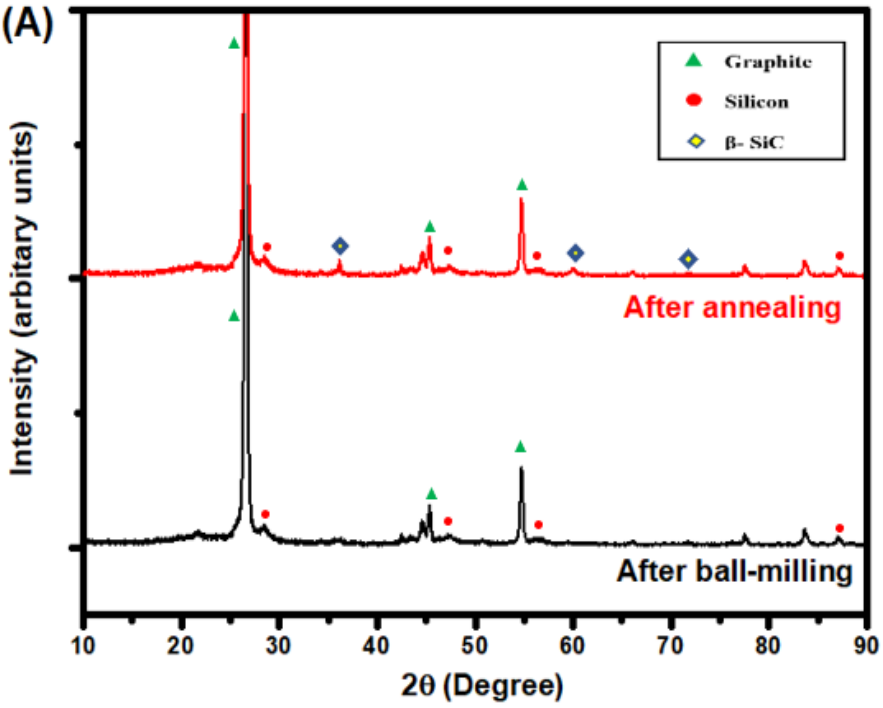

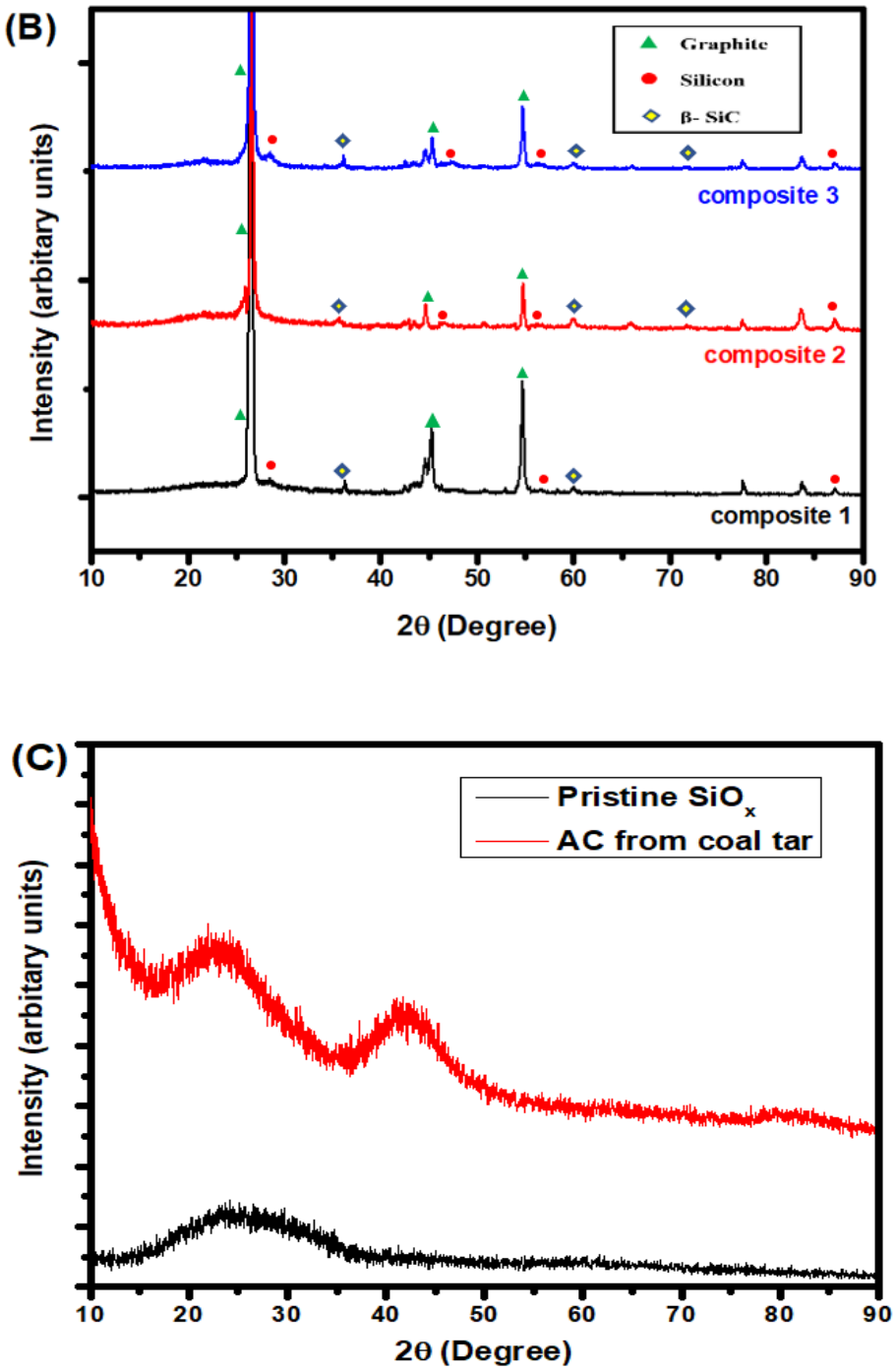

Figure 26: XRD characterization of the as-prepared composite materials (A) XRD analysis of composite 3 after the two-step mechanical ball-milling and after thermal annealing at 1000℃ (B) XRD analysis of the as-prepared composite materials after thermal annealing at 1000℃ (C) XRD analysis of the pristine SiO_x and AC derived from annealing coal tar at 1000℃.

Figure 27 shows the TGA curves for the as-prepared composite materials after the two-step process of dual mechanical milling followed by thermal annealing at 1000℃. The measurements were taken between 80℃ and 900℃ under air flow (0.06 L/min) at a heating rate of 10℃/min. As the composites consists majorly of graphite, a typical TGA curve pertaining to NFG is observed. The composites retained most of its original weight (100%) till about 550℃ after which it showed a rapid loss of weight till 800℃. This drop started from 550℃ and is attributed to the combustion reaction of graphite, other volatiles and O_2 .[65] Post 900℃, the composites 1, 2 and 3 retained 16%, 34% and 38% of its original weight respectively. The weight loss was primarily the sum total weight % of the graphite present in the samples, and the weight retained post 900℃ was the resultant free Si and SiCNWs left in the composite matrix. Due to the presence of a higher amount of SiCNWs, a temperature delay before the onset of weight loss by combustion was also noticed for the TGA curves of composites 2 and 3, adding to the stability to the composite. On the contrary, the TGA curve of composite 1, having a very high graphite content (80%) and a relatively small amount of SiCNW formation, exhibited substantial weight loss right from 150℃.

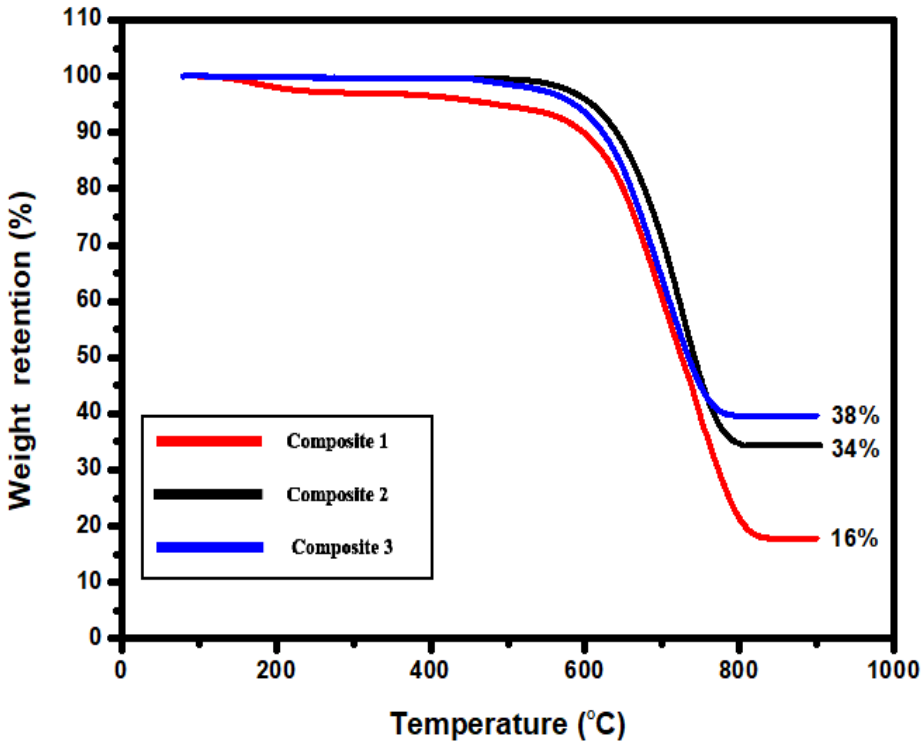

Figure 27: TGA curves of the as-prepared composites between 80°C and 900°C under air flow at a heating rate of 10°C/min.

SEM characterization was done to investigate the morphology of the various as-prepared composites. Although the exact microstructure of the commercial SiO_x was not known to be reported ,[66-67] a model was later proposed which described the SiO_x as nano-clusters of Si and SiO_2 in a sub-oxide matrix.[62] These agglomerated and clustered SiO_x particles were very distinctly observed across the composite matrix in the SEM images in Figure 28(a). The two-step ball-milling process not only helps in the uniform distribution of the Si/SiO_x particles over the graphite matrix, but also reduces the large pristine graphite particles from 10-20 microns to 5-10 microns and the pristine SiO_x from 15-30 microns to micro-nano sized Si/SiO_x particles ranging between 200 nm to a few microns. The use of ammonium bicarbonate as a leavening agent shows its effect

by the presence of pores and hollow spaces that are formed as a result of CO_2 and NH_3 gas formation from the heating of the ammonium bicarbonate salt.[68] These empty spaces between the successive graphite and SiO_x particles throughout the matrix potentially accommodates the volume expansion and swelling of the adjoining Si/SiO_x particles during the subsequent cycling process. Figure 28(b) shows a section of a typical SiCNW-Si/SiO_x-graphite composite depicting the presence of a micro-cluster of Si/SiO_x particles entrapped in the graphite matrix. A closer investigation of these clusters in Figure 28(c) confirm the presence of uniformly dispersed spherical Si NPs having poly dispersion with sizes ranging between 40 nm-70 nm.[69-71] Figure 28(d) also depicts a cluster of Si/SiO_x in the composite matrix corresponding to composite 3.

The EDS elemental mapping analysis technique was carried out with an aim to map carbon, oxygen and silicon for the SEM image shown in Figure 28(d) and the elemental overlay mapping was obtained and presented in Figure 29(a) by superimposing the individual mapping images of carbon, oxygen and silicon in Figure 29(b)-(d) respectively. The overall mapping showed a very uniform distribution of the SiO_x in a unique architecture in which the clusters of micro-nano sized Si/SiO_x particles comprising of nano-silicon in a sub-oxide matrix were seen surrounded by graphite on all sides. This nature is also seen previously in Figure 28(d) and we can infer that the as-prepared composite materials possess this unique trait wherein the SiO_x particles consisting of Si NPs in the sub-oxide matrix cluster together to form micro-nano sized particles that are evenly dispersed throughout the graphite matrix. As discussed previously, the Si NPs were well dispersed in the SiO_x matrix on subjecting the composites to thermal annealing at 1000℃ and also as a result of the disproportionation reactions on milling the SiO_x with coal tar.[56-58] This unique architecture thereby serves as an excellent buffer to accommodate the volume change of the SiO_x particles during the subsequent lithiation and de-lithiation cycles.

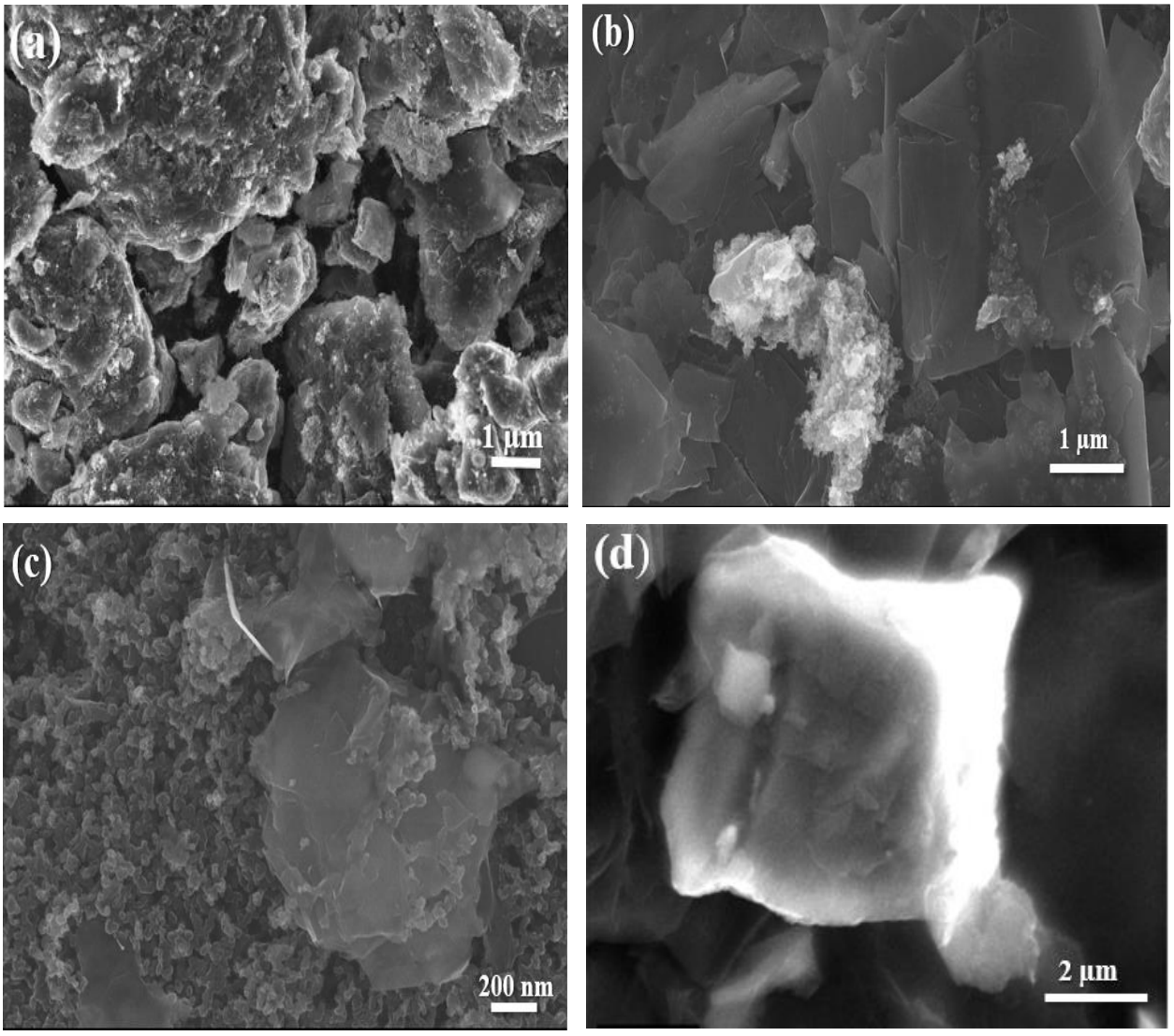

Figure 28:(a) -(d) SEM characterization images for a typical section of a SiCNW-Si/SiOx-graphite composite material (composite 3).

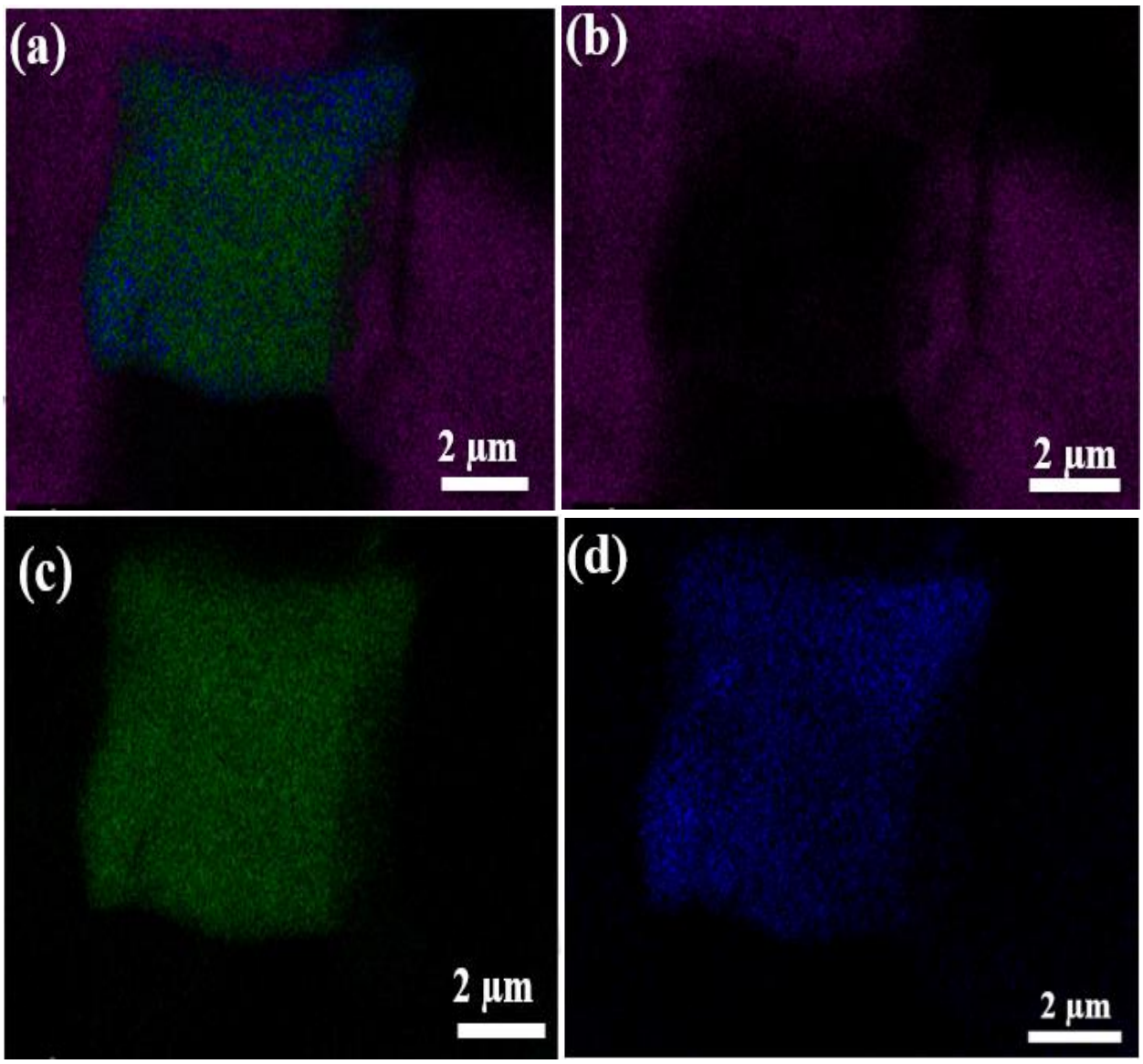

Figure 29: EDS mapping images for SEM image shown in Fig 28(d) (a) elemental overlay mapping image for carbon, oxygen and Si (b) EDS mapping image for carbon (c) EDS mapping image for Si and (d) EDS mapping image for oxygen.

Figure 30 (a)-(b) illustrate the SEM images of a section of composite 2 and composite 3 respectively, depicting the distinct presence of uniformly distributed micro-nano sized Si/SiOx

particles and thread like SiCNWs throughout the graphite framework. These nanowires were found to be nanowires of β-SiC, which were formed via a two-step growth mechanism. Firstly, as a result of the mechanical milling of SiO_x with coal tar (carbon source), a mixture of micro-nano sized Si/SiO_x particles alongside smaller SiO_x particles covered with a thin layer of coal tar were formed. On thermal annealing at 1000℃, the coal tar covered SiO_x particles self-assembled to form a number of highly curled nanoparticle chains. By the increasing the temperature and duration of annealing, the coal tar converted to amorphous carbon, which eventually diffused into the Si lattice to react with the Si particles to form numerous thread like β-SiCNWs.[60] To further investigate and establish these findings alongside the unique composite structure, TEM characterization was performed on composites 2 and 3 and the images illustrated through Figure 30(c)-(d). Dark crystalline nano-Si "spots" ranging between 50-100 nm were observed in both these figures, while clustered micro-nano sized Si/SiO_x particles were observed on the transparent sheet like graphite structure in Figure 30(c). The Si nanoparticles were seen encapsulated and surrounded by multiple overlapping graphite sheets. Figure 30(c) also shows the distinct presence of curled "curtain-bead like" SiCNWs.[42] As explained previously, these nanowires were formed by a two-step self growth mechanism resulting from the combined effects of the mechanical milling and annealing process. These SiCNWs were seen to possess a diameter of roughly 70-100 nm and ranged between few nanometers to several microns in length. The presence of these thread like SiCNWs and micro-nano sized Si/SiO_x clusters are also observed in the remaining composite materials. These findings are in tune with our previous findings from the SEM characterization and EDS elemental mapping technique and provide a better insight in understanding the unique architecture of the as-prepared composites.

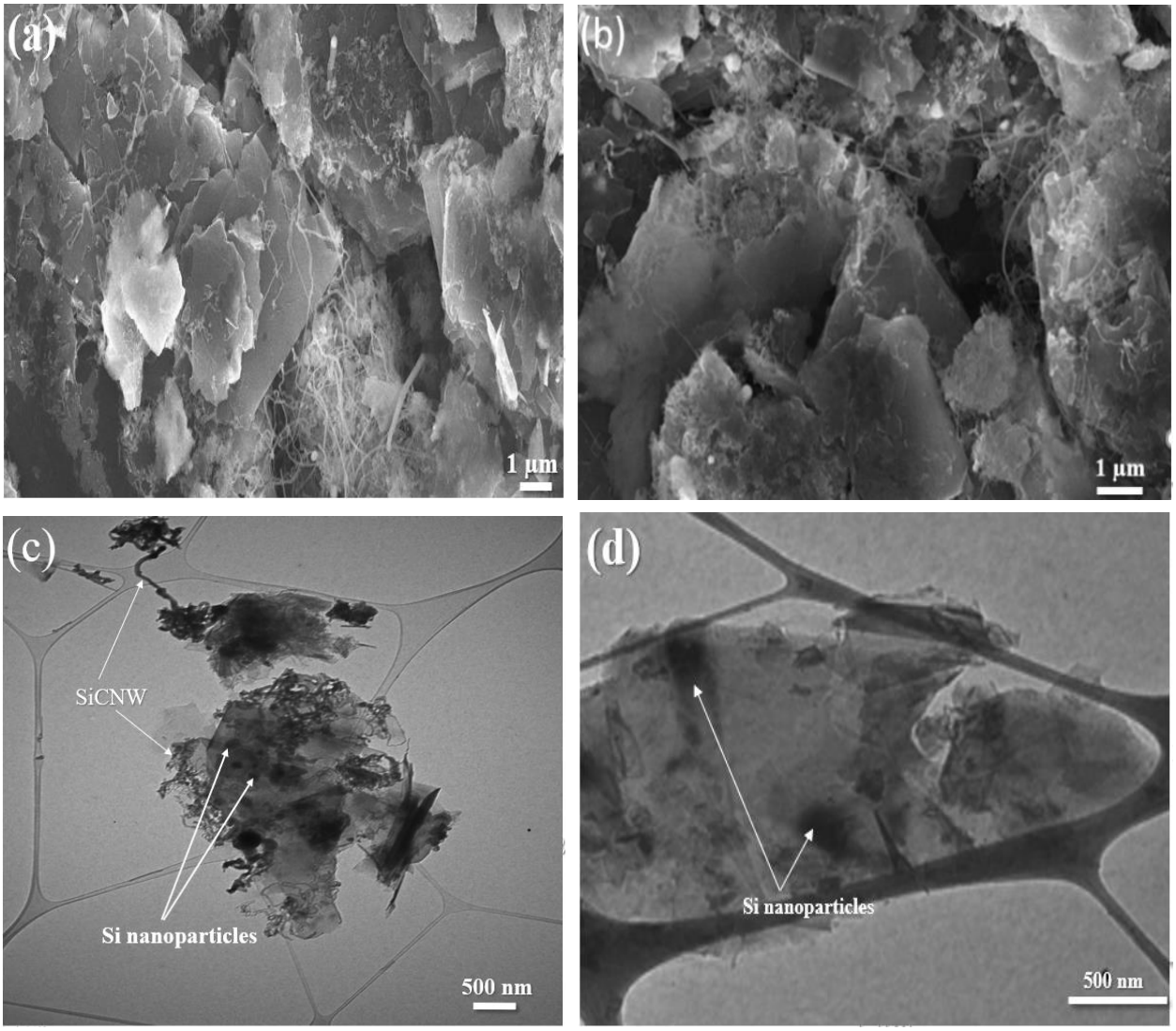

Figure 30: (a) -(b) SEM characterization image of a section of composite 2 and composite 3 showing the presence of SiCNWs and Si/SiOx particles in the graphite matrix (c)TEM characterization image of a section of composite 2 showing the distinct presence of curled SiCNWs and Si NPs spread across the graphite matrix (d)TEM characterization image for a section of composite 3 showing the presence of Si NPs encapsulated in the graphite matrix.

The electrochemical characteristics and performance of the as-prepared composites were tested separately as an anode material for lithium-ion batteries by testing it in coin-type half-cells against lithium metal as the counter electrode. Figure 31 illustrates the galvanostatic charge/discharge curves for the first cycle for each of the three composites at a rate of 0.1 A/g between the voltage window of 0.01V-1.5V. The first cycle discharge and charge capacities of composite 1 were 702 mAh/g and 548.9 mAh/g respectively, corresponding to a first cycle coulombic efficiency of 78.2%. The first cycle discharge and charge values for composite 2 were found to be 894.3 mAh/g and 610.1 mAh/g corresponding to a coulombic efficiency of 68.3%, and those of composite 3 were 1143.9 mAh/g and 868 mAh/g, corresponding to a first cycle coulombic efficiency of 75.8%.

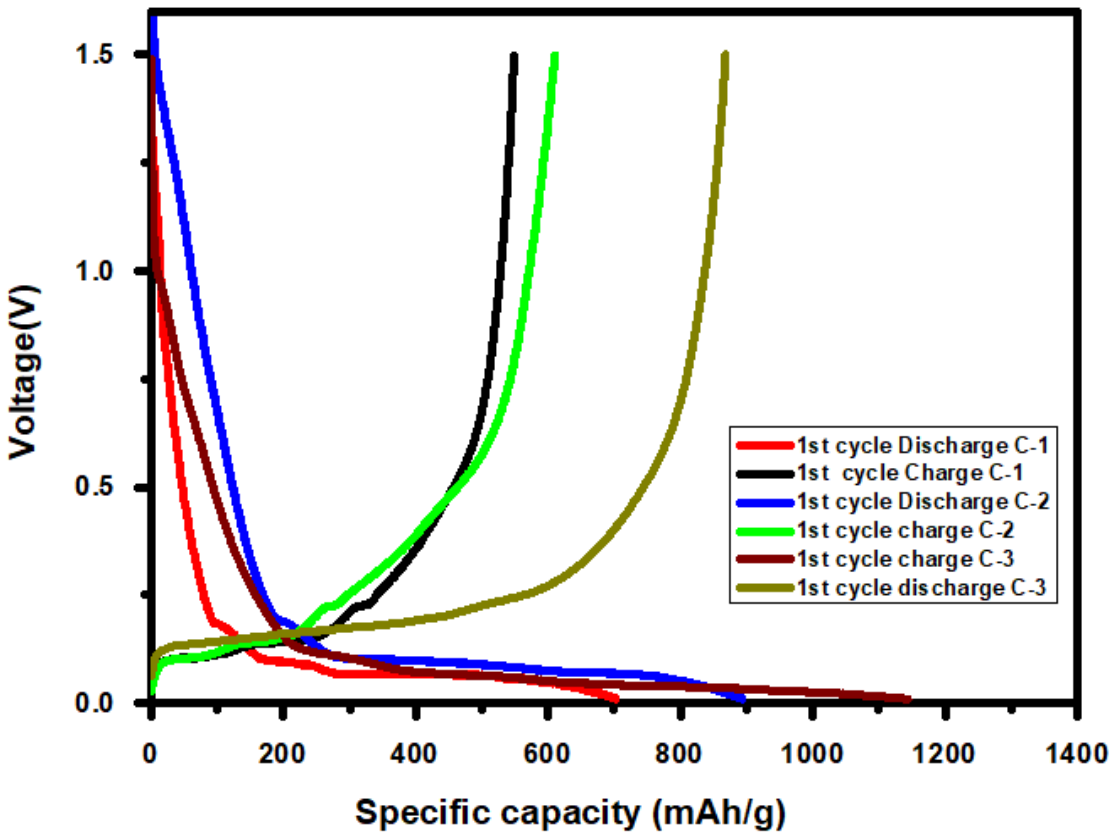

Figure 31: 1st cycle charge-discharge profile at 0.1 A/g for the three composites.

Figure 32 shows the rate capability of the composites cycled at varying rates ranging between 0.1-2A/g. All the cells showed good stability and capacity retention as the cells stabilized just after a few cycles at higher rate values. The cells of composite 1 showed reversible capacities of 575.2 mAh/g, 475 mAh/g, 330 mAh/g, 225.4 mAh/g and 170 mAh/g when cycled at 0.05 A/g, 0.25 A/g, 0.5 A/g, 1A/g and 2 A/g respectively, compared to 632 mAh/g, 535 mAh/g, 375 mAh/g, 260 mAh/g and 210 mAh/g for composite 2 and 880 mAh/g, 740 mAh/g, 690 mAh/g, 545 mAh/g and 370 mAh/g for composite 3 respectively. Upon reverting the current rate back to 0.1 A/g, the cell regained its capacity with an increased capacity showing the excellent stability of the composite.

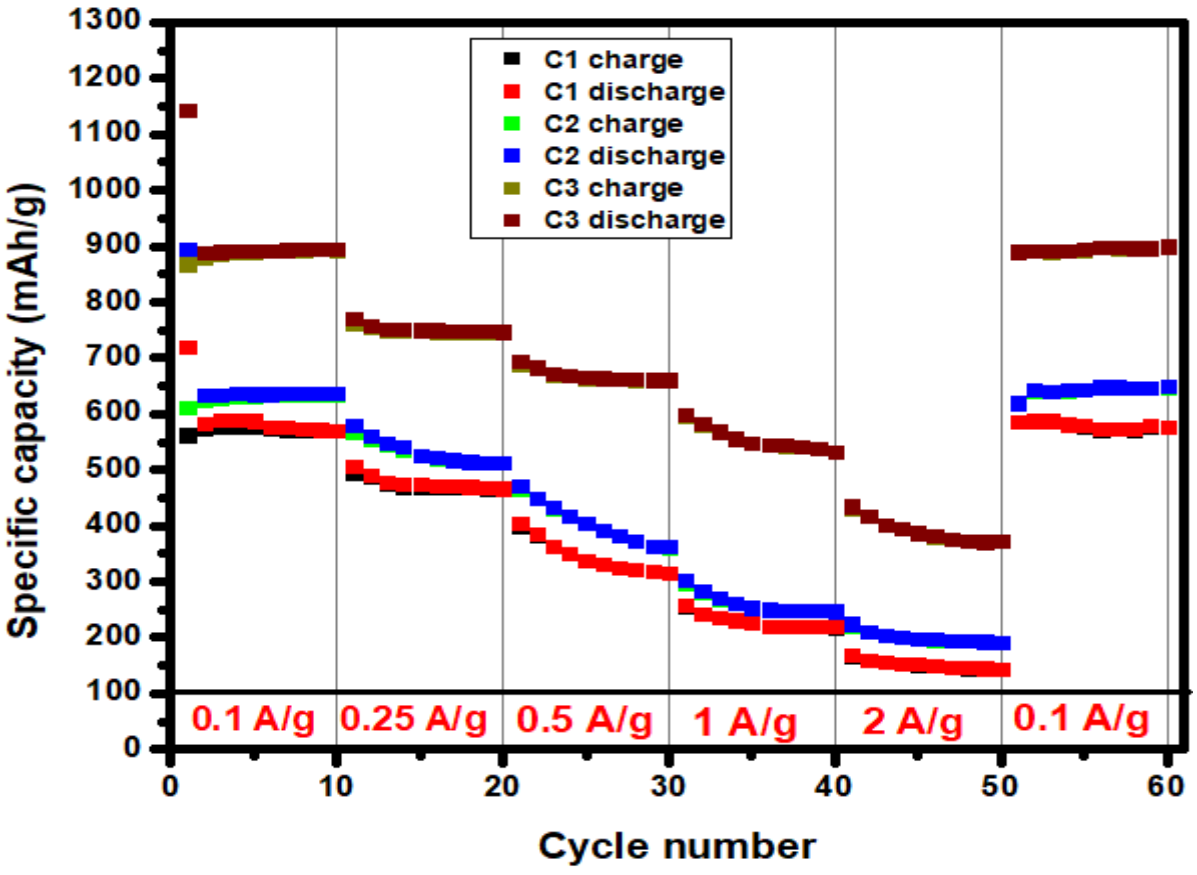

Figure 32: Rate capability test at varying rates between 0.1-2 A/g for the three composites.

The long-term cycling was carried out for each of the cells at a rate of 0.1 A/g for 500 cycles and the combined results are illustrated in Figure 33. All the cells exhibited stable performance and good capacity retention with consistently high coulombic efficiency (99.75% at the end of fourth cycle and stable at ~99.87% for 500 cycles) at the end of 500 cycles. Composite 3 retained a very high reversible capacity of 760 mAh/g at the end of 500 cycles at 0.1 A/g corresponding to a remarkable capacity retention of 87.6% at the end of 500 cycles ,when compared to its first cycle charge capacity of 868 mAh/g. Composite 2 retained a capacity of 508 mAh/g after 500 cycles corresponding to a capacity retention of 83.2% ,when compared to its first cycle capacity of 610.7 mAh/g and composite 1 yielded a remarkable capacity retention of 91.3% corresponding to a capacity of 500.1 mAh/g at the end of 500 cycles when compared to its 1st cycle charge capacity of 548 mAh/g.

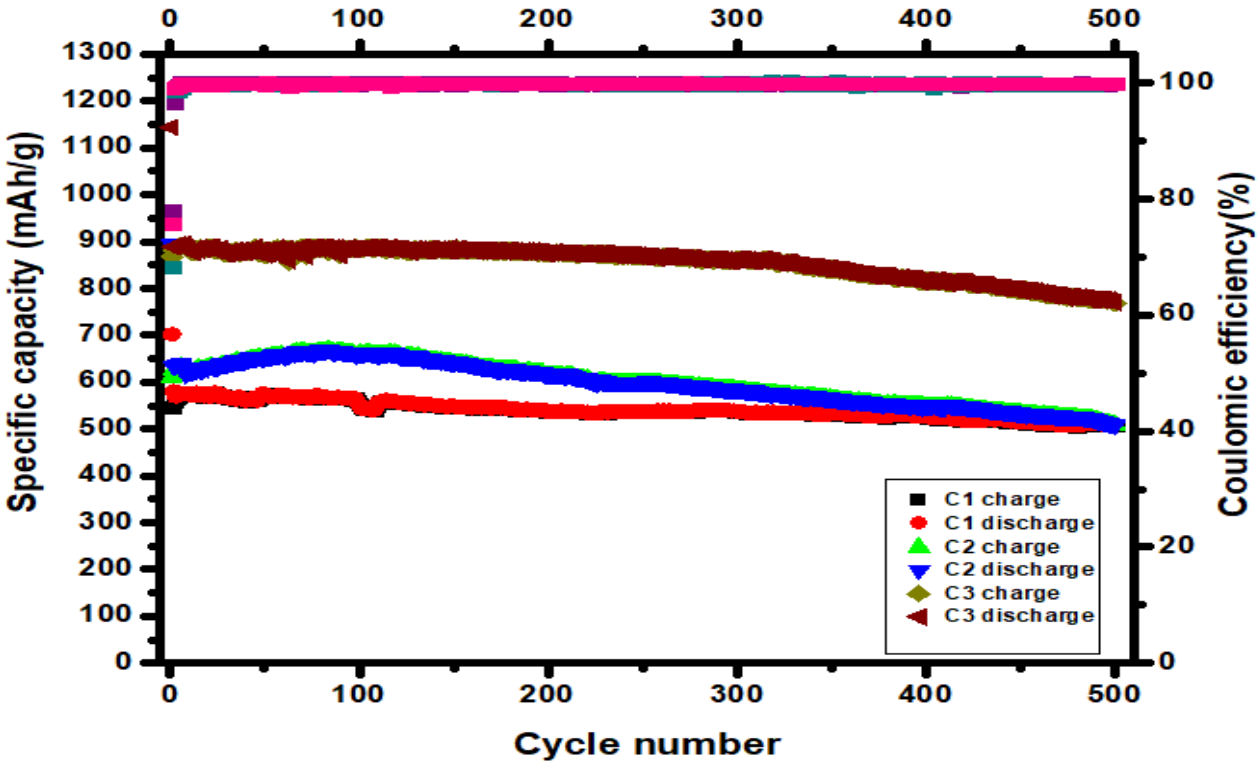

Figure 33: Long-term cycle performance at 0.1 A/g for 500 cycles for the three composites.

On a comparative point of view, composite 1 gives the maximum first cycle coulombic efficiency (78.2%) followed by composite 3 (75.8%) and composite 2 (68.3%) respectively. The high coulombic efficiency of composite 1 can be attributed to its high graphite content (80%). Although composite 2 and composite 3 both contain the same amount of graphite by weight (60%), they differ substantially in their SiO_x and coal tar amounts. Composite 2, which has a lower SiO_x content (20%) but relatively higher coal tar content (16%) forms a larger amount of SiCNWs post annealing, compared to composite 3 having 25 % SiO_x and 11% coal tar. The presence of SiC is known to lead to a higher irreversible capacity loss and low first cycle efficiency.[39-40] It is for this reason composite 2 shows a lower coulombic efficiency of 68.3% compared to 75.8% for composite 3. Composite 3, on the other hand shows the maximum initial cycle discharge and charge capacities of 1143.9 mAh/g and 868 mAh/g respectively. This can once again be explained by the varying quantity of graphite, SiO_x and coal tar in the composites. While the increase in graphite reduces the capacity of the overall composite, the free Si within the Si/SiO_x particles increases the capacity. But with the increase in coal tar amount, more Si is actively taken up by the coal tar to form complete SiC particles.[72] Hence composite 2 has a much higher SiCNW formation and a low amount of free Si in the composite matrix (4%) compared to composite 3 which has an optimum amount of SiCNW formation coupled with a much higher free Si content (14%) in the matrix .A distinct feature noticed in all the three composite electrodes was that there was a gradual increase in capacity in the first few cycles, which is attributed to the activation reaction of β-SiC nanowires. Afterwards, a gradual slow decay in capacity is observed over cycling owing to structural changes in long cycle time.[42] It is for this very reason that we earlier noticed in Figure 33 that composite 2 exhibited a sudden drastic increase in charge capacity from the very first cycle and the capacity increased steadily until the 83rd cycle to 668 mAh/g, after which the

capacity started dropping gradually .This was in tune with our previous findings for the rate capability test of composite 2 in Figure 32, wherein the composite showed a gradual increase in capacity upon reverting the rate back to 0.1 A/g. The increase in capacity of the composites highlights the successful accommodation of the volume change of the Si/SiO_x particles within the composite matrix. From the cyclability point of view, all the three composites show remarkable stability, but composite 1 shows the best capacity retention of 91.3% followed by composite 3 (87.6 %) and composite 2 (83.2%). This can again be well explained by the varying amounts of free Si, SiCNWs and graphite present in the composites. While a large amount of graphite is imperative for the long cycle stability of the composites, an optimal coal tar amount is required to maintain good conductivity of the composite coupled with a higher amount of free Si to achieve a higher reversible capacity. With the increase in coal tar, more SiC particles are formed, eventually leading to increased formation of β-SiC nanowires and lesser available free Si in the composite (in the form of the Si/SiO_x particles), as Si is used up to form the SiC nanowires. While composite 2 has a relatively higher coal tar content, but a lesser free Si available (4%) coupled with a higher SiCNW formation, slightly lowered its long-term capacity retention to 83.2% as compared to the rest. Composite 1 having the advantage of the maximum graphite content (80%) and a low SiC nanowire and free Si content, exhibited remarkable stability with a capacity retention of 91.3% after 500 cycles at 0.1 A/g, but with a much lower reversible capacity. Composite 3 although having a lower graphite content (60%), enjoys the supreme advantage of an optimal amount of SiCNW and high free Si content. This coupled effect enables composite 3 to show a remarkable capacity retention of 87.6% with a very high reversible capacity of 760 mAh/g after 500 charge-discharge cycles at 0.1A/g, in spite of having a low graphitic and high Si content in the original state. The superior cycle stability of composite 3 over composite 2 can also be attributed to the

higher remaining SiO_x. According to previous findings by researchers, the presence of a surface layer of SiOx on Si, plays an important role of enhancing the stability of the Si particles on long cycling.[81-82] Hence composite 3 has a superior capacity retention post 500 charge-discharge cycles, as compared to composite 2, although composite 2 has a much higher amount of SICNW formation .SiCNWs are known to possess a variety of desirable characteristics like high thermal stability, inertness to chemical attack, chemical resistivity, hardness, high mechanical strength.[60,73-74] They have hence been previously used as an effective buffer to accommodate the volume change of Si-based anode materials and as an effective backbone to enhance the electronic conductivity of various composite materials.[75-77] With the optimum amount of β-SiC nanowires, coupled with a high free Si available in the composite matrix, composite 3, delivered a high capacity with superior cycling performance and increased conductivity, while effectively buffering the volume change of the Si/SiO_x particles and preventing capacity fading by disintegration of active material by imparting strength to the composite electrode.

Figure 34(A)-(C) shows the cyclic voltammetry (CV) curves for cells of the as-prepared composites, between the voltage window of 0.01-1.5 V at a scan rate of 0.1 mV/s for the first three cycles. For the first cycle, a peak was observed at around 1.13V for composite 1, which can be associated with the electrolyte decomposition and formation of the SEI layer from EC based electrolytes.[78] This also highlights the fact that the composite forms a smooth and stable SEI layer on the first cycle and this peak completely fades in the following cycles. The sharp cathodic peaks close to the cut-off potential, i.e. between 0-0.25V ascribe to the lithiation reactions of silicon and graphite in the composite, resulting in the formation of amorphous Li_xSi and Li_xC. The cathodic peak centered at 0.19 V is due to the formation of the metastable Li_xSi. This peak appeared in the very first cycle for composite 2 and 3 and was not observed in the first scan for composite 1. It

appeared subsequently after the second cycle for composite 1, marking the onset of the Li_xSi phase. The cathodic peak at 0.01V was ascribed to the lithiation reaction of graphite to form Li_xC. The delithiation occurred at approximately 0.50 V as lithium ions were extracted from Li_xSi alloy to form amorphous Si. Interestingly, this peak was only observed for composite 3 after the end of the very first cycle itself, primarily owing to the increased active Si content in composite 3 as compared to the rest as discussed before. The intensity of this peak became more pronounced with increased scan times and number of cycles due to the increased activation of the Si phase alongside an enhanced electronic kinetics process.[79] It is evident from literature that the reversible lithiation of the β-SiC does not involve the formation of "definite potential-dependent phases" meaning the SiC does not disintegrate into its constituents and the CV or voltage profile show the evident formation of Li_xSi and Li_xC phase.[41] Our findings corroborate with literature since no additional peaks other than those ascribing to the lithiation and delithiation of Si and graphite are seen in the CV curves for the three composites. This also highlights the fact that the broad peak at 0.50 V is due to the formation of amorphous Si from the available free silicon in the composite and not from the β-SiCNWs. The anodic peaks near 0.25 V can be ascribed to the formation of amorphous C phase after lithium extraction from Li_xC.[78,80-82] No significant shift was observed in the CV curves in the subsequent scans and the shape of the CV curve for the composites changed to a lesser extent, portraying that the reversibility of Li insertion and extraction in the composite was improved substantially, leading to superior cycling performance in the subsequent cycles.

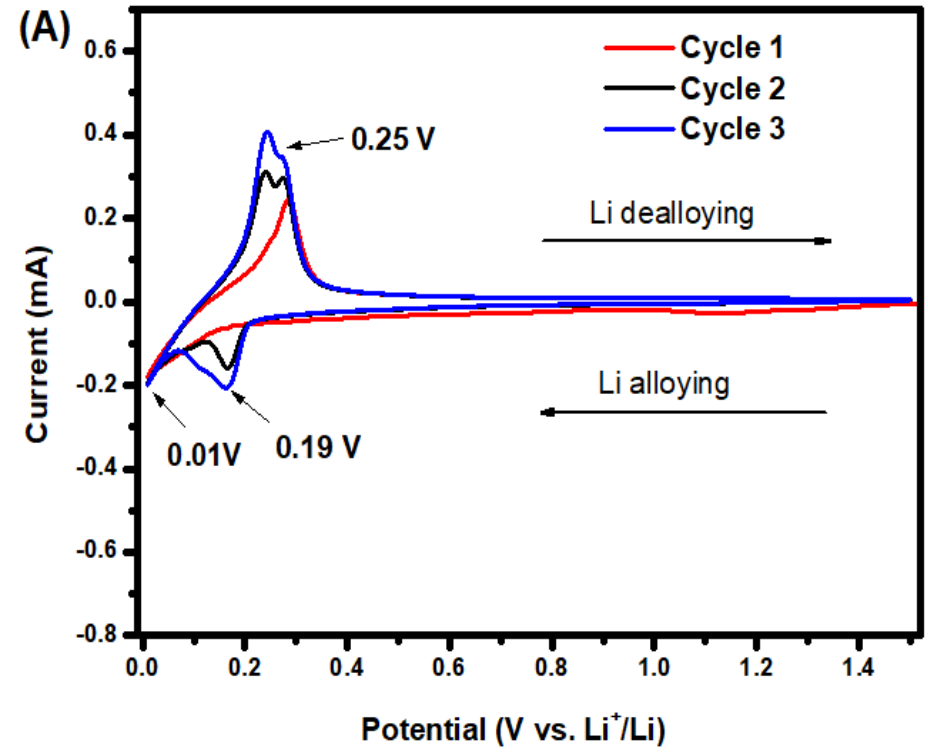
(A)
Cycle 1
Cycle 2
Cycle 3
0.25 V
Li dealloying
Li alloying
0.01V
0.19 V
Current (mA)
Potential (V vs. Li+/Li)

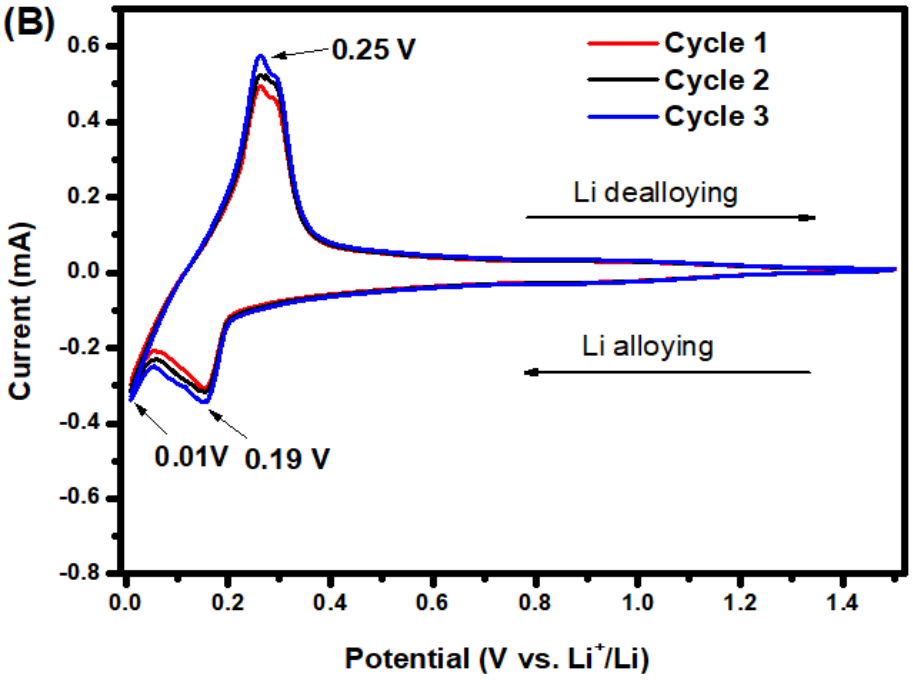
(B)
Cycle 1
Cycle 2
Cycle 3
0.25 V
Li dealloying
Li alloying
0.01V
0.19 V
Current (mA)
Potential (V vs. Li+/Li)

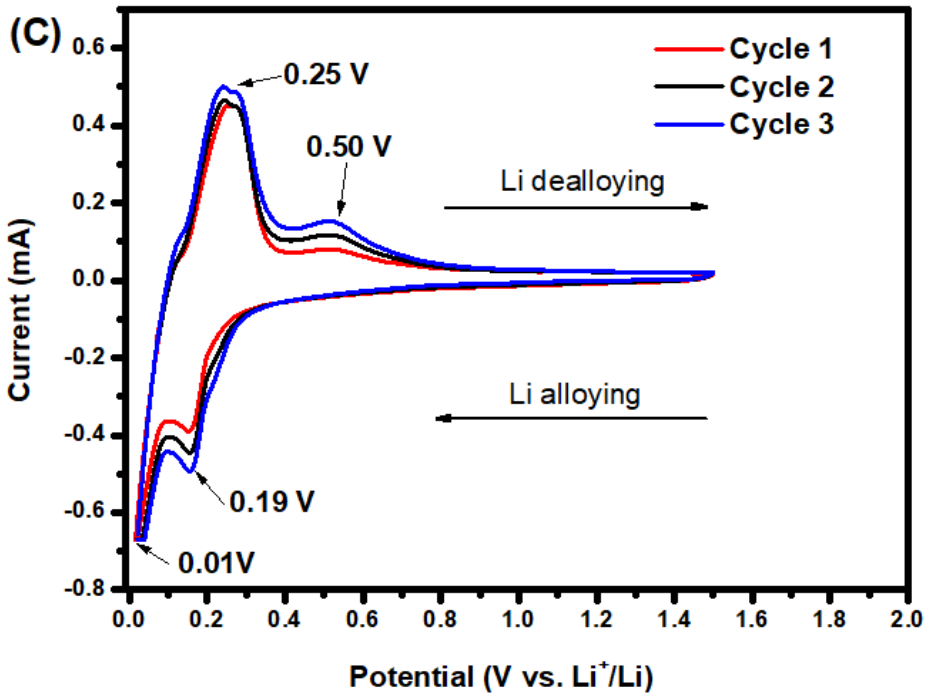

Figure 34:Cyclic voltammetry curves of the composite cells for the first three cycles, at a scan rate of 0.1 mV/s (A) composite 1(B) composite 2 and (C) composite 3.

5.4 Conclusion

In summary, SiCNW-Si/SiOx-graphite composites were synthesized from bulk SiO_x , NFG powder, and coal tar as an effective carbon precursor, via a cost-effective facile synthesis process comprising of a mechanical ball-milling operation followed by thermal annealing of the as-prepared composites at 1000°C in an inert argon atmosphere. The as-prepared composite materials possessed a unique architecture of micro-nano sized Si/SiO_x clustered particles and thread-like SiCNWs homogeneously dispersed and encapsulated within a conductive graphite matrix. This unique architecture could effectively buffer the volume expansion of the Si/SiOx particles during the subsequent charge/discharge process. When used as an anode material in a LIB, these

composites exhibited high capacity, superior stability and remarkable cyclic retention, alongside a remarkable electrochemical performance. The SiCNWs in the composite maintained the structural integrity of the composite electrodes thereby preventing the mechanical disintegration and loss of active electrode material over the repeated charge/discharge process. This process not only opens up an economic yet simple way to produce highly stable composites, which can potentially replace graphite as the next generation anode material for LIB application, but also presents a new facile economical route for the production of SiCNWs.

6.0 Summary and future work

The anode is a crucial component of the LIB. As discussed previously, the challenge is that none of the existing anode materials completely meet all the required performance characteristics. These criterions include a high capacity, good rate performance, good stability, a higher operating voltage and a long cycle life. Hence extensive research is focused on finding novel hybrid anode materials that deliver good cycle performance, high energy and power density and long cycle life, which will allow LIBs to be implemented into the EV industry. Herein, the electrochemical performance of pristine natural graphite and SiO_x was first tested as an anode material for LIB. On one hand, the NFG electrodes exhibited a good cyclability with good long-term stability and capacity retention of 80% at 0.5 C post 200 charge-discharge cycles. The SiO_x on the other hand, exhibited a very poor cyclability and lost almost 50% of its initial capacity in a mere 20 cycles when cycled at 0.5 C.

It was previously established from the first project that graphite was a bottleneck when it came to delivering a higher specific capacity and SiO_x was a bottleneck in delivering an improved cycle life. This spurred the very need and idea to create a composite anode material that delivers on both a higher specific capacity and a stable cycle life and performance. Thus, in the composite project, by incorporating graphite and SiO_x in the same cell, SiCNW-Si/SiOx-graphite composites were synthesized from bulk SiO_x and NFG powder alongside coal tar as an effective carbon precursor, via a cost-effective facile synthesis process comprising of a mechanical ball-milling operation followed by thermal annealing of the as-prepared composites at 1000℃ in an inert argon atmosphere.

The as-prepared composite materials were seen to possess a unique architecture of micro-nano sized Si/SiO_x clustered particles and thread-like SiCNWs homogeneously dispersed and encapsulated within a conductive graphite matrix. This unique architecture could effectively buffer the volume expansion of the Si/SiOx particles during the subsequent charge/discharge process. When used as an anode material in a LIB, these composites exhibited a high specific capacity, superior stability and remarkable cyclic retention alongside remarkable electrochemical performance. The presence of SiCNWs in the composite maintained the structural integrity of the composite electrodes thereby preventing the mechanical disintegration and loss of active electrode material over the repeated charge/discharge process. This process not only opens up an economic yet simple way to produce highly stable composites, which can potentially replace graphite as the next generation anode material for LIB application, but also presents a new facile economical route for the production of SiCNWs for a variety of applications.

Although several promising results were obtained in the projects, there is an ample room for improvement. The composite project delivered composites with a much higher specific capacity (760 mAh/g post 500 cycles) than that of its graphite counterpart. But is possible to deliver an anode with a much higher specific capacity. Although the use of SiO_x instead of Si in this project, could explain the lower capacity of the composites as compared to Si. But with the incorporation of Si, it is indeed possible to obtain composites with a much higher specific capacity as Si has a theoretical capacity of 4200 mAh/g. Extensive research work should be carried out on Si-based anodes which use a higher amount of Si to achieve a higher capacity coupled with improved cycle life and rate performance. It is a major challenge to researchers across the globe for achieving this, primarily owing to the poor cycle life and capacity fading of Si-based anodes resulting from the volume expansion of the Si particles on repeated cycling coupled with its poor conductivity.

However, it is possible to alleviate this volume expansion by several techniques, one such being the formation of core-shell Si/C composites that could potentially accommodate the volume change of the Si particles on repeated cycling. Other techniques like the incorporation of an inactive phase with Si, pyrolysis with numerous carbon-based materials and engineering the morphology and structure of the Si anode has a promising future in the application of the ever-growing LIB industry.

References

1 Nitta, N., Wu, F., Lee, J. T., & Yushin, G. Li-ion battery materials: Present and future. *Materials Today*.,18(5) (2015), 252-264.

2 Etacheri, V., Marom, R., Elazari, R., Salitra, G., & Aurbach, D. Challenges in the development of advanced Li-ion batteries: a review. *Energy & Environmental Science*, *4*(9) (2011), 3243–3262.

3 Armand, M., & Tarascon, J.-M. Building better batteries. *Nature*, *451*(7179) (2008), 652–657.

4 Scrosati, B., & Garche, J. Lithium Batteries: Status, Prospects and Future. *J. Power Sources*, *195*(9) (2010), 2419–2430.

5 Thackeray, M. M., Wolverton, C., Isaacs, E. D., Winter, M., Brodd, R. J., Tarascon, J. M, Sun, Y. K. Electrical energy storage for transportation approaching the limits of, and going beyond, lithium-ion batteries. *Energy & Environmental Science*, *5*(7) (2012),7854-7863.

6 Manthiram, A. Materials Challenges and Opportunities of Lithium Ion Batteries. *The Journal of Physical Chemistry Letters*, *2*(3) (2011), 176–184.

7 Choi, N., Chen, Z., Freunberger, S. A., Ji, X., Sun, Y., Amine, K., Yushin, G., Nazar, L. F., Cho, J. and Bruce, P. G. Challenges Facing Lithium Batteries and Electrical Double-Layer Capacitors. *Angew. Chem. Int. Ed*., 51(2012), 9994-10024.

8 Oh, J., Jin, D., Kim, K., Song, D., Lee, Y. M., & Ryou, M.H. Improving the Cycling Performance of Lithium-Ion Battery Si/Graphite Anodes Using a Soluble Polyimide Binder. *ACS Omega*, *2*(11) (2017), 8438–8444.

9 Whittingham, M. S. Materials challenges facing electrical energy storage. *MRS Bulletin*, *33*(4) (2008), 411–419.

10 Goodenough, J. B., & Kim, Y. Challenges for Rechargeable Li Batteries. *Chemistry of Materials*, *22*(3) (2010), 587–603.

11 Natarajan, C., Fujimoto, H., Tokumitsu, K., Mabuchi, A., & Kasuh, T. Reduction of the irreversible capacity of a graphite anode by the CVD process. *Carbon*, *39*(9) (2001), 1409–1413.

12 Yoshio, M., Wang, H. and Fukuda, K., Spherical Carbon-Coated Natural Graphite as a Lithium-Ion Battery-Anode Material. *Angewandte Chemie International Edition*, 42(2003), 4203-4206.

13 Guoping, W., Bolan, Z., Min, Y., Xiaoluo, X., Meizheng, Q., & Zuolong, Y. A modified graphite anode with high initial efficiency and excellent cycle life expectation. *Solid State Ionics*, *176*(9) (2005), 905–909.

14 Wang, F., Li, W., Hou, M., Li, C., Wang, Y., & Xia, Y. Sandwich-like Cr_2O_3-graphite intercalation composites as high-stability anode materials for lithium-ion batteries. *J. Mater. Chem. A*, *3*(4) (2015), 1703-1708.

15 Lee, M.L., Li, Y.H., Liao, S.C., Chen, J.M., Yeh, J.W., & Shih, H. C. $Li_4Ti_5O_{12}$-coated graphite as an anode material for lithium-ion batteries. *Applied Surface Science, 258*(16) (2012), 5938–5942.

16 Lin, Y., Huang, Z.H., Yu, X., Shen, W., Zheng, Y., & Kang, F. Mildly expanded graphite for anode materials of lithium ion battery synthesized with perchloric acid. *Electrochimica Acta*, *116*(2014), 170–174.

17 Chai, L., Qu, Q., Zhang, L., Shen, M., Zhang, L., & Zheng, H. Chitosan, a new and environmental benign electrode binder for use with graphite anode in lithium-ion batteries. *Electrochimica Acta*, *105*(2013), 378–383.

18 Si, Q., Hanai, K., Ichikawa, T., Hirano, A., Imanishi, N., Takeda, Y., & Yamamoto, O. A high-performance silicon/carbon composite anode with carbon nanofiber for lithium-ion batteries. *Journal of Power Sources*, *195*(6) (2010), 1720–1725.

19 J. M. Tarascon and M.Armand, Issues and challenges facing rechargeable lithium batteries. *Nature*, 414 (2001), 359-367.

20 Bruce, P. G., Scrosati, B., & Tarascon, J. M. Nanomaterials for rechargeable lithium batteries. *Angew Chem Int Ed Engl*. 47 (2008),2930-2946.

21 Yushin, G., Magasinski, A., Dixon, P., Hertzberg, B., Kvit, A., & Ayala, J. High-performance lithium-ion anodes using a hierarchical bottom-up approach. *Nature Materials*, *9*(4) (2010), 353–358.

22 M. Yoshio, T. Tsumura, N. Dimov.J. Electrochemical behaviors of silicon based anode material. *Journal of Power Sources* 146 (2005) 10-14.

23 Key, B., Bhattacharyya, R., Morcrette, M., Seznec, V., Tarascon, J. M., & Grey, C. P..Real-Time NMR Investigations of Structural Changes in Silicon Electrodes for Lithium-Ion Batteries. *Journal of the American Chemical Society*, *131*(26) (2009), 9239–9249.

24 Jeong, G., Kim, J.-H., Kim, Y.-U., & Kim, Y.-J. Multifunctional TiO_2 coating for a SiO anode in Li-ion batteries. *J. Mater. Chem.*, *22*(16) (2012), 7999–8004.

25 Miyachi, M., Yamamoto, H., Kawai, H., Ohta, T., & Shirakata, M. Analysis of SiO Anodes for Lithium-Ion Batteries. *Journal of The Electrochemical Society*, *152*(10) (2005), A2089.

26 H. Lee, S. Lee. Silicon Based Composite Anode for Lithium Ion Battery. *Electrochemistry Communications* 6 (2004),465–469.

27 Tomokazu, M., Norio, T. Nano Si Cluster-SiO_x-C Composite Material as High-Capacity Anode Material for Rechargeable Lithium Batteries. Journal of the Electrochemical Society, 153 (2006), A425–A430.

28 Kim, J.H., Sohn, H.J., Kim, H., Jeong, G., & Choi, W. Enhanced cycle performance of SiO-C composite anode for lithium-ion batteries. *Journal of Power Sources*, *170*(2) (2007), 456–459.

29 Yang, X., Wen, Z., Xu, X., Lin, B., & Huang, S. Nanosized silicon-based composite derived by in situ mechanochemical reduction for lithium ion batteries. *Journal of Power 164(2)* (2007), 880–884.

30 Levi, M. D., & Aurbach, D. Diffusion Coefficients of Lithium Ions during Intercalation into Graphite Derived from the Simultaneous Measurements and Modelling of Electrochemical Impedance and Potentiostatic Intermittent Titration Characteristics of Thin Graphite Electrodes. *The Journal of Physical Chemistry B*, *101*(23) (1997), 4641–4647.

31 Bard, A.J, Faulkner, L.F. Electrochemical Methods – Fundamentals and Applications. *Wiley, New York 85*(11) (1980), 1085–1086.

32 Lee, J.I., & Park, S. High-performance porous silicon monoxide anodes synthesized via metal-assisted chemical etching. *Nano Energy*, *2*(1) (2013), 146–152.

33 Guerfi, A., Charest, P., Dontigny, M., Trottier, J., Lagacé, M., Hovington, P., Zaghib, K. SiO_x-graphite as negative for high energy Li-ion batteries. *Journal of Power Sources, 196*(13) (2011), 5667-5673.

34 Datta, M. K., & Kumta, P. N. Silicon and carbon based composite anodes for lithium ion batteries. *Journal of Power Sources*, *158*(1) (2006),557–563.

35 Doh, C.H., Park, C.W., Shin, H.M., Kim, D.H., Chung, Y.D., Moon, S.I., Veluchamy, A. A new SiO/C anode composition for lithium-ion battery. *Journal of Power Sources*, *179*(1) (2008), 367–370.

36 Wang, Y.X., Chou, S.L., Kim, J. H., Liu, H.-K., & Dou, S.X. Nanocomposites of silicon and carbon derived from coal tar pitch: Cheap anode materials for lithium-ion batteries with long cycle life and enhanced capacity. *Electrochimica Acta*, *93*(2013), 213–221.

37 Wen, Z. S., Yang, J., Wang, B. F., Wang, K., & Liu, Y. High capacity silicon/carbon composite anode materials for lithium ion batteries. *Electrochemistry Communications*, *5*(2) (2003), 165–168.

38 Han, Y.J., Kim, J., Yeo, J.S., An, J. C., Hong, I.P., Nakabayashi, K., Yoon, S.H. Coating of graphite anode with coal tar pitch as an effective precursor for enhancing the rate performance in Li-ion batteries: Effects of composition and softening points of coal tar pitch. *Carbon*, *94*(2015), 432–438.

39 Son, I. H., Park, J. H., Kwon, S., Park, S., Rümmeli, M. H., Bachmatiuk, A., Chang, H.Silicon carbide-free graphene growth on silicon for lithium-ion battery with high volumetric energy density. *Nature Communications*, *6* (2015),7393.

40 Datta, M. K., & Kumta, P. N. Silicon, graphite and resin based hard carbon nanocomposite anodes for lithium ion batteries. *Journal of Power Sources*, *165*(1) (2007), 368–378

41 Sri Devi Kumari, T., Jeyakumar, D., & Prem Kumar, T. Nano silicon carbide: a new lithium-insertion anode material on the horizon. *RSC Adv.*, *3*(35) (2013), 15028–15034.

42 Hu, Y., Liu, X., Zhang, X., Wan, N., Pan, D., Li, X., Zhang, W. Bead-curtain shaped SiC@SiO_2 core-shell nanowires with superior electrochemical properties for lithium-ion batteries. *Electrochimica Acta*, *190* (2016), 33–39.

43 Si, Q., Hanai, K., Ichikawa, T., Hirano, A., Imanishi, N., Takeda, Y., & Yamamoto, O. A high-performance silicon/carbon composite anode with carbon nanofiber for lithium-ion batteries. *Journal of Power Sources*, *195*(6) (2010), 1720–1725.

44 J. M. Tarascon and M.Armand, Issues and challenges facing rechargeable lithium batteries. *Nature*, 414 (2001), 359-367.

45 Bruce, P. G., Scrosati, B., & Tarascon, J. M. Nanomaterials for rechargeable lithium batteries. *Angew Chem Int Ed Engl*. 47 (2008),2930-2946.

46 Yushin, G., Magasinski, A., Dixon, P., Hertzberg, B., Kvit, A., & Ayala, J. High-performance lithium-ion anodes using a hierarchical bottom-up approach. *Nature Materials*, *9*(4) (2010), 353–358.

47 M. Yoshio, T. Tsumura, N. Dimov.J. Electrochemical behaviours of silicon-based anode material. *Journal of Power Sources* 146 (2005) 10-14.

48 Key, B., Bhattacharyya, R., Morcrette, M., Seznec, V., Tarascon, J. M., & Grey, C. P. Real-Time NMR Investigations of Structural Changes in Silicon Electrodes for Lithium-Ion Batteries. *Journal of the American Chemical Society*, *131*(26) (2009), 9239–9249.

49 Gallego, N. C., Contescu, C. I., Meyer, H. M., Howe, J. Y., Meisner, R. A., Payzant, E. A. Wood, D. L. Advanced surface and microstructural characterization of natural graphite anodes for lithium ion batteries. *Carbon*, *72*(2014), 393–401.

50 Lee, J.I., & Park, S. High-performance porous silicon monoxide anodes synthesized via metal-assisted chemical etching. *Nano Energy*, *2*(1) (2013), 146–152.

51 Hohl, A., Wieder, T., van Aken, P. A., Weirich, T. E., Denninger, G., Vidal, M., Fuess, H. An interface clusters mixture model for the structure of amorphous silicon monoxide (SiO). *Journal of Non-Crystalline Solids*, *320*(1) (2003), 255–280.

52 Yu, B.C., Hwa, Y., Kim, J.-H., & Sohn, H.J. A New Approach to Synthesis of Porous SiO_x Anode for Li-ion Batteries via Chemical Etching of Si Crystallites. *Electrochimica Acta*, *117*(2014), 426–430.

53 Gallego, N. C., Contescu, C. I., Meyer, H. M., Howe, J. Y., Meisner, R. A., Payzant, E. A. Wood, D. L. Advanced surface and microstructural characterization of natural graphite anodes for lithium ion batteries. *Carbon*, *72*(2014), 393–401.

54 Li, M., Zeng, Y., Ren, Y., Zeng, C., Gu, J., Feng, X., & He, H. Fabrication and lithium storage performance of sugar apple-shaped SiOx@C nanocomposite spheres. Journal of Power Sources, 288(2015), 53–61.

55 Schulmeister, K., & Mader, W. TEM investigation on the structure of amorphous silicon monoxide. *Journal of Non-Crystalline Solids*, *320*(1–3) (2003), 143–150.

56 Wang, J., Zhou, M., Tan, G., Chen, S., Wu, F., Lu, J., & Amine, K. Encapsulating micro-nano Si/SiOx into conjugated nitrogen-doped carbon as binder-free monolithic anodes for advanced lithium ion batteries. *Nanoscale*, *7*(17) (2015), 8023–8034.

57 Feng, X., Yang, J., Lu, Q., Wang, J., & Nuli, Y. Facile approach to SiOx/Si/C composite anode material from bulk SiO for lithium ion batteries. *Phys. Chem. Chem. Phys.*, *15*(34) (2013), 14420–14426.

58 Park, C. M., Choi, W., Hwa, Y., Kim, J.-H., Jeong, G., & Sohn, H.-J. Characterizations and electrochemical behaviours of disproportionated SiO and its composite for rechargeable Li-ion batteries. *J. Mater. Chem.*, *20*(23) (2010), 4854–4860.

59 Lee, J.I., & Park, S. High-performance porous silicon monoxide anodes synthesized via metal-assisted chemical etching. *Nano Energy*, *2*(1) (2013), 146–152.

60 Kang, P., Zhang, B., Wu, G., Gou, H., Chen, G., Jiang, L., & Mula, S. Synthesis of β-SiC nanowires by ball milled nanoparticles of silicon and carbon. *Journal of Alloys and Compounds*, *604*(2014), 304–308.

61 Lee, J.I., & Park, S. High-performance porous silicon monoxide anodes synthesized via metal-assisted chemical etching. *Nano Energy*, *2*(1) (2013), 146–152.

62 Hohl, A., Wieder, T., van Aken, P. A., Weirich, T. E., Denninger, G., Vidal, M., Fuess, H. An interface clusters mixture model for the structure of amorphous silicon monoxide (SiO). *Journal of Non-Crystalline Solids*, *320*(1) (2003), 255–280.

63 Yu, B.C., Hwa, Y., Kim, J.-H., & Sohn, H.J. A New Approach to Synthesis of Porous SiO_x Anode for Li-ion Batteries via Chemical Etching of Si Crystallites. *Electrochimica Acta*, *117*(2014), 426–430.

64 Wang, Y., Xiao, N., Wang, Z., Li, H., Yu, M., Tang, Y., Qiu, J. Rational design of high-performance sodium-ion battery anode by molecular engineering of coal tar pitch. *Chemical Engineering Journal*, *342*(2018), 52–60.

65 Cataldo, F. A study on the thermal stability to 1000 ℃ of various carbon allotropes and carbonaceous matter both under nitrogen and in air. *Fullerenes Nanotubes and Carbon Nanostructures*, *10*(4) (2002), 293–311.

66 Füglein, E., & Schubert, U. Formation of Mg_2Si from Solid Silicon Monoxide, and Solid-State Comproportionation between Mg_2Si and SiO. *Chemistry of Materials*, *11*(4) (1999), 865–866.

67 Philipp, H. R. Optical properties of non-crystalline Si, SiO, SiO_x and SiO_2. *Journal of Physics and Chemistry of Solids*, *32*(8) (1971), 1935–1945.

68 Miller, R. Leavening Agents. *Encyclopedia of Food and Health* ,1 (2016),523–528.

69 Lee, J.H., Kim, W.J., Kim, J.Y., Lim, S.H., & Lee, S.M. Spherical silicon/graphite/carbon composites as anode material for lithium-ion batteries. *Journal of Power Sources*, *176*(1) (2008), 353–358.

70 Hovington, P., Dontigny, M., Guerfi, A., Trottier, J., Lagacé, M., Mauger, A., Zaghib, K. In situ Scanning electron microscope study and microstructural evolution of nano silicon anode for high energy Li-ion batteries. *Journal of Power Sources*, *248*(2014), 457–464.

71 Sun, W., Hu, R., Zhang, H., Wang, Y., Yang, L., Liu, J., & Zhu, M. A long-life nano-silicon anode for lithium ion batteries: supporting of graphene nanosheets exfoliated from expanded graphite by plasma-assisted milling. *Electrochimica Acta*, *187*(2016), 1–10.

72 Zhang, G., Wei, G., Zheng, K., Li, L., Xu, D., Wang, D., Su, W. The Synthesis of beta-SiC Nanoparticles by High-Energy Mechanical Ball Milling and Their Photoluminescence Properties. *Journal of Nanoscience and Nanotechnology*, *10(3) (2010),*1951–1955.

73 Wong, E. W., Sheehan, P. E., & Lieber, C. M. Nanobeam mechanics: Elasticity, strength, and toughness of nanorods and nanotubes. *Science*, *277*(5334) (1997), 1971–1975.

74 Inagaki, M., & Kang, F. *Materials Science and Engineering of Carbon: Fundamentals*. *Materials Science and Engineering of Carbon: Fundamentals*. 2 (2014),17-217.

75 Jeon, B. J., & Lee, J. K. Electrochemical characteristics of nc-Si/SiC composite for anode electrode of lithium ion batteries. *Journal of Alloys and Compounds*, *590*(2014), 254–259.

76 Wang, C., Li, Y., Ostrikov, K. (Ken), Yang, Y., & Zhang, W. Synthesis of SiC decorated carbonaceous nanorods and its hierarchical composites Si@SiC@C for high-performance lithium ion batteries. *Journal of Alloys and Compounds*, *646*(2015), 966–972.

77 Wang, W., Wang, Y., Gu, L., Lu, R., Qian, H., Peng, X., & Sha, J. SiC@Si core–shell nanowires on carbon paper as a hybrid anode for lithium-ion batteries. *Journal of Power Sources*, *293*(2015), 492–497.

78 Ren, Y., & Li, M. Si-SiOx-Cristobalite/Graphite Composite as Anode for Li-ion Batteries. *Electrochimica Acta*, *142*(2014), 11–17.

79 Chou, S.L., Wang, J.Z., Choucair, M., Liu, H.K., Stride, J. A., & Dou, S.X. Enhanced reversible lithium storage in a nanosize silicon/graphene composite. *Electrochemistry Communications*, *12*(2) (2010)., 303–306.

80 Li, J., Wang, J., Yang, J., Ma, X., & Lu, S. Scalable synthesis of a novel structured graphite/silicon/pyrolyzed-carbon composite as anode material for high-performance lithium-ion batteries. *Journal of Alloys and Compounds*, *688*(2016), 1072–1079.

81 Xin, X., Zhou, X., Wang, F., Yao, X., Xu, X., Zhu, Y., & Liu, Z. A 3D porous architecture of Si/graphene nanocomposite as high-performance anode materials for Li-ion batteries. *J. Mater. Chem.*, *22*(16) (2012), 7724–7730.

82 Zhang, T., Gao, J., Zhang, H. P., Yang, L. C., Wu, Y. P., & Wu, H. Q. Preparation and electrochemical properties of core-shell Si/SiO nanocomposite as anode material for lithium ion batteries. *Electrochemistry Communications*, *9*(5) (2007)., 886–890.